NASA TECHNICAL MEMORANDUM

NASA TM X-2353

CALIBRATION OF THE LANGLEY MACH 20 HIGH REYNOLDS NUMBER HELIUM TUNNEL INCLUDING DIFFUSER MEASUREMENTS

by Ralph D. Watson and Dennis M. Bushnell

Langley Research Center
Hampton, Va. 23365

NATIONAL AERONAUTICS AND SPACE ADMINISTRATION • WASHINGTON, D. C. • OCTOBER 1971

1. Report No.	2. Government Accession No.	3. Recipient's Catalog No.
NASA TM X-2353		

4. Title and Subtitle	5. Report Date
CALIBRATION OF THE LANGLEY MACH 20 HIGH REYNOLDS NUMBER HELIUM TUNNEL INCLUDING DIFFUSER MEASUREMENTS	October 1971
	6. Performing Organization Code

7. Author(s)	8. Performing Organization Report No.
Ralph D. Watson and Dennis M. Bushnell	L-7756
	10. Work Unit No.
9. Performing Organization Name and Address	136-63-03-01
NASA Langley Research Center Hampton, Va. 23365	11. Contract or Grant No.
	13. Type of Report and Period Covered
12. Sponsoring Agency Name and Address	Technical Memorandum
National Aeronautics and Space Administration Washington, D.C. 20546	14. Sponsoring Agency Code

15. Supplementary Notes

16. Abstract

Detailed flow characteristics in the Mach 20 leg of the Langley high Reynolds number helium tunnels have been determined for stagnation pressures from 207 to 1379 N/cm^2 (300 to 2000 psia) at ambient stagnation temperature. For this range of stagnation pressure the free-stream Mach number varies from 16.7 to 18.4 in the Reynolds number range from 7.6×10^6 to 48.6×10^6 per meter (2.3×10^6 to 14.8×10^6 per ft). The axial Mach number gradient has been found to be 0.125 per meter (0.038 per ft) and the inviscid core approximately 50.8 cm (20 in.) in diameter with a probable length of 1060 cm (417 in.). Nondimensional radial distributions of Mach numbers are similar to distributions obtained previously in the Langley 22-inch helium tunnel. Pressures measured along the sidewall of the diffuser are presented and analyzed to determine flow conditions within the diffuser as back pressure rises during a run. These flow conditions were determined to insure that undue loads due to unusual flow conditions were not placed on a large butterfly valve downstream of the diffuser.

17. Key Words (Suggested by Author(s))	18. Distribution Statement
Tunnel calibration Mach 20 helium tunnel	Unclassified – Unlimited

19. Security Classif. (of this report)	20. Security Classif. (of this page)	21. No. of Pages	22. Price*
Unclassified	Unclassified	42	$3.00

*For sale by the National Technical Information Service, Springfield, Virginia 22151

CALIBRATION OF THE LANGLEY MACH 20 HIGH REYNOLDS NUMBER HELIUM TUNNEL INCLUDING DIFFUSER MEASUREMENTS

By Ralph D. Watson and Dennis M. Bushnell
Langley Research Center

SUMMARY

Detailed flow characteristics in the Mach 20 leg of the Langley high Reynolds number helium tunnels have been determined for stagnation pressures from 207 to 1379 N/cm^2 (300 to 2000 psia) at ambient stagnation temperature. For this range of stagnation pressure the free-stream Mach number varies from 16.7 to 18.4 in the Reynolds number range from 7.6×10^6 to 48.6×10^6 per meter (2.3×10^6 to 14.8×10^6 per ft). The axial Mach number gradient has been found to be 0.125 per meter (0.038 per ft) and the inviscid core approximately 50.8 cm (20 in.) in diameter with a probable length of 1060 cm (417 in.). Nondimensional radial distributions of Mach numbers are similar to distributions obtained previously in the Langley 22-inch helium tunnel. Pressures measured along the sidewall of the diffuser are presented and analyzed to determine flow conditions within the diffuser as back pressure rises during a run. These flow conditions were determined to insure that undue loads due to unusual flow conditions were not placed on a large butterfly valve downstream of the diffuser.

INTRODUCTION

Within the past 20 years, the hypersonic helium tunnel has proved to be a valuable tool in aerodynamic research. Early tunnels, such as those at Princeton University and Langley Research Center, had test sections only a few cm in diameter (see refs. 1 and 2), although later ones ranged up to 56 cm (22 in.) in size. Some new tunnels have been designed for extremely high Mach numbers, for example, the Ames Mach 50 helium tunnel described in reference 3 and the Langley Mach 40 helium tunnel recently completed but not yet operational. The tunnel described in this report is the Mach 20 leg of the high Reynolds number helium tunnels at Langley Research Center. The test section is 152.4 cm (60 in.) in diameter with a usable core about 50.8 cm (20 in.) in diameter and a maximum Reynolds number capability of 96.4×10^6 per meter (29.4×10^6 per ft).

The most frequently cited advantage of using helium as the test medium is that Mach numbers as high as 35 can be achieved without liquefaction in unheated flow (e.g., see

ref. 4). The advantages of using unheated flow at hypersonic speeds include not only a saving in heater and facility design costs but simplification in instrumentation setups in that delicate instruments do not have to be cooled.

In addition, unheated helium has the advantage of generating significantly higher Reynolds numbers than air at the same stagnation pressure and Mach number. As noted in reference 5, helium is a "benign medium" for studying turbulence at hypersonic speeds using hot-wire techniques. Also, the recent development of electron-beam flow visualization (ref. 6) in helium tunnels has proved valuable in the visualization of complex three-dimensional flow-field interactions, such as those encountered with conceptual space-shuttle configurations. In addition to being useful as a general hypersonic tool, the facility described in this report, because of its large size and high Reynolds number, allows the detailed study of transitional and turbulent flows on models (rather than model walls) at Mach numbers greater than 10.

The present report presents detailed calibration and diffuser measurements in the Mach 20 leg of the Langley high Reynolds number helium tunnels.

SYMBOLS

Values are given in both the International System of Units (SI) and U.S. Customary Units. The measurements and calculations were made in the U.S. Customary Units.

d	nozzle throat diameter
D	diffuser diameter
M	Mach number
p	pressure
r	local radial distance measured from tunnel center line
R	local radial distance from tunnel center line to wall
t	time
T	temperature
x	axial distance measured from nozzle throat

x' axial distance measured from beginning of test section

x_d axial distance measured from beginning of diffuser

δ boundary-layer thickness determined from pitot survey

δ^* boundary-layer displacement thickness

ϕ angle measured as shown in figure 4

Subscripts:

c average value within a 25.4-cm-diameter (10-in.) circle

s value in vacuum sphere

t stagnation-chamber value

w value at nozzle wall

∞ free-stream value

¢ center-line value

DESCRIPTION OF FACILITY

The Langley high Reynolds number helium tunnels consist of Mach 10 and Mach 20 legs (nozzles, test sections, and diffusers) operating from a 56.6 m^3 (2000 ft^3) high-pressure storage supply and exhausting into two 18.3-meter-diameter (60-ft) vacuum spheres. Vacuum pumps, a seven-stage compressor, and a purifier are common to both legs. Figure 1 shows a schematic of the closed-cycle operation of the Mach 10 and 20 legs. Two pressure vessels, each of 28.3 m^3 (1000 ft^3) capacity, permit helium storage at any desired pressure up to 4551 N/cm^2 (6600 psia). At present, the tunnels are limited to a maximum stagnation pressure of 1379 N/cm^2 (2000 psia) for unheated flow; however, in future operations, this will be extended to 2758 N/cm^2 (4000 psia). The present report will consider only data from the Mach 20 leg. A typical maximum run time for the Mach 20 leg is 6 seconds, essentially independent of stagnation pressure. This 6-second run time includes an initial startup period of approximately 1 second during which the stagnation pressure increases to the value specified for the run.

Figure 2(a) shows the wall coordinates of the Mach 20 contoured nozzle designed for $p_t = 2758$ N/cm^2 (4000 psia), $T_t = 294^o$ K (530^o R), and $T_w = 294^o$ K (530^o R). Calculations were made using a computer program similar to that described in reference 7. An inviscid core was calculated assuming source flow in region BC and a linear Mach number distribution from B to A. Then a boundary-layer displacement thickness calculated by the method of Persh and Lee (ref. 8) was added to the core to determine the wall coordinates. Nozzle cutoff length was determined by the method of reference 9 with $\delta/\delta^* = 2$, a value which has been shown in reference 10 to be characteristic of hypersonic turbulent boundary layers on tunnel walls in helium flow.

The inviscid region for a design Mach number of 20 is not shown in figure 2(a). An inviscid core at $M = 18$ was calculated to match measured free-stream conditions at stagnation pressures near 1379 N/cm^2 (2000 psia). The displacement thickness was assumed to be the difference between this core and the nozzle wall. An estimate of the pitot boundary-layer thickness was made by doubling δ^* and subtracting the result from the nozzle wall. Reasonable agreement between the thickness estimated by this method and that determined from the data of figure 6 is shown in figure 2(a). Note that the final Mach line CD predicts a uniform core extending about 762 cm (300 in.) ahead of the test section.

Dimensions of the test section, diffuser, and model support mounts are shown in figure 2(b). Also shown are the locations of 11 pressure taps used for measuring static pressures along the diffuser. A photograph of the test section is shown in figure 3.

INSTRUMENTATION AND DATA REDUCTION

Survey Rakes and Transducers

Two rakes were used for Mach number surveys in the test section; rake A had a 10.2-cm (4-in.) radial tube spacing for coarse surveys, and rake B, a 2.54-cm (1-in.) radial tube spacing for detailed surveys in a 25.4-cm-diameter (10-in.) section of the core. Sketches of the two rakes are shown in figure 4. The fine rake had a nine-tube arm for definition of the boundary-layer edge in addition to the core tubes. The outside diameter of the tubes was 0.318 cm (0.125 in.) for both rakes.

Stagnation pressures, pitot pressures, and diffuser pressures were measured by strain-gage transducers. Transducer ranges were selected to give an accuracy in pressure measurements of approximately 1 percent. Data were recorded on a 100-channel analog-to-digital converter and tape recorder. A limit of 56 strain-gage transducers which can be recorded at one time for any one facility connected to the digitizer; however, 100 channels of thermocouple data can be recorded. Overall accuracy in the resulting calculated Mach number is estimated to be 1 percent. Wall static pressures were measured

with variable-capacitance transducers. Vibration in the vacuum isolation valve was measured with a torsigraph and with strain gages bonded to the valve shaft.

Total temperature is measured in the stagnation chamber with unshielded 24-gage iron-constantan thermocouples. The free-stream total temperature measured with a shielded 0.32-cm-diameter (1/8-in.) probe and the total temperature in the stagnation chamber are shown in figure 5. The temperature peak which occurs at 0.2 to 0.3 second after the start of the run is due to the quick start of the tunnel instead of real-gas expansion effects. After steady flow with constant stagnation pressure has been achieved (i.e., after about 1 sec), the free-stream total temperature is higher than the stagnation-chamber temperature by approximately the value predicted in reference 4.

Data-Reduction Procedures

In reducing measured values of pitot and stagnation pressure to Mach number, the ideal-gas tabulations of reference 11 were used, modified by the real-gas correction factors of reference 12 which are necessary because of the deviation of helium from the ideal-gas law at high stagnation pressures. In addition to high-pressure real-gas corrections, low-temperature quantum effects on viscosity discussed in reference 13 are applied to free-stream Reynolds numbers quoted in this report.

RESULTS AND DISCUSSION

Mach Number Surveys

Mach number surveys at nominal stagnation pressures of 207, 345, 483, 689, 1034, and 1379 N/cm^2 (300, 500, 700, 1000, 1500, and 2000 psia) were made at the following four stations in the test section: station 1, $x' = 30.15$ cm (11.87 in.); station 2, $x' = 80.95$ cm (31.87 in.); station 3, $x' = 182.5$ cm (71.85 in.); and station 4, $x' = 284.1$ cm (111.85 in.). Additional surveys were obtained at stagnation pressures of 69 and 827 N/cm^2 (100 and 1200 psia). Pitot pressures from rake A were divided by the corrected value of p_t for a given run to calculate the Mach number distributions which are shown in the upper part of figure 6 (looking downstream). Mach numbers calculated from tubes in regions of nonisentropic flow (i.e., in the boundary layer at the tunnel wall or behind shocks in the flow) would appear too high when calculated from the ratio of pitot pressure to stagnation pressure. The lower part of figure 6 shows a radial Mach number distribution calculated from the ratio of pitot pressure to free-stream static pressure. The pitot pressures were obtained from the outer tubes of rake A and the boundary-layer arm of rake B. This arm was located at a 45^o angle in the upper left quadrant looking downstream, as indicated in figure 4. Free-stream static pressure was calculated by using an average Mach number determined from the core data obtained with the fine rake.

Detailed Mach number distributions in a 25.4-cm-diameter (10-in.) core obtained from the fine rake are shown in figure 7. A fairing of the data at each tunnel position and pressure is indicated in the figure. These average Mach numbers are plotted as a function of p_t in figure 8 for various tunnel stations and exhibit the usual trend of increasing Mach number with increasing p_t. Figure 9 shows the longitudinal variation of average core Mach numbers for various stagnation pressures; the data show a linear Mach number gradient of 0.125 per meter (0.038 per ft), nearly invariant with stagnation pressure.

A summary of the capabilities of the Mach 20 leg of the Langley high Reynolds number helium tunnels is given in table I.

The radial Mach number distributions in the Langley 22-inch helium tunnel and in the Mach 20 leg of the Langley high Reynolds number helium tunnels are shown in figure 10 at an x/d value of 215. The Mach number data plotted as a function of r/R show that the ratio of core radius to test-section radius is approximately the same in both tunnels. Center-line-region disturbances having the same magnitude are also present in both tunnels. Deviations of the center-line Mach number from M_c are plotted against x' at various stagnation pressures in figure 11. It appears that with increasing stagnation pressure, the maximum deviation increases slightly and the location of the maximum disturbance moves downstream. This downstream movement is in agreement with inviscid-core calculations at Mach numbers of 18 and 20. These calculations show that if the throat diameter is held fixed, the origin of the final Mach line moves downstream as free-stream Mach number is increased. Thus, it is probable that the free-stream disturbances may be generated in one region of the nozzle, but the flow is affected in the test section at different locations, dependent on the tunnel stagnation pressure. Reference 14 notes that the region of maximum expansion in the nozzle (shown in fig. 2(a)) is the approximate point of origin of such disturbances.

Nozzle-Wall Pressure Measurements

Measurements of wall static pressure were made at a position 61 cm (24 in.) upstream of the function of the nozzle and the test section at $\phi = 0^\circ$ and 180°. (See fig. 4 for ϕ convention.) Free-stream static pressure at the same point was calculated by extrapolating M_c from figure 9, using the ideal-gas ratios from reference 11, and applying the real-gas corrections of reference 12. Ratios of p_w/p_∞ were formed for comparison with the correlation of reference 9, where it was shown that significant increases in p_w/p_∞ are obtained at hypersonic Mach numbers when the boundary layer is turbulent. Reference 9 notes that fluctuating normal velocities in turbulent boundary layers could possibly give rise to this effect.

The resulting ratio varies between 0.8 and 0.9, whereas reference 9 predicts a ratio of about 1.3. Pressures had settled out for each run and four different gages were used in

order to eliminate gage calibration errors. Reasons for the discrepancy between measured and theoretical values are not known at this time. Possible explanations are that the extrapolation of M_c may not be accurate; that is, disturbances may exist in the flow upstream of the survey station, or that higher Mach numbers downstream may influence the pressure measurements upstream.

Diffuser Measurements

Static pressures along diffuser.- For each run, pressures were measured at 11 locations along the side of the diffuser. The results for a typical run are shown in figure 12 at various times during the run. The diffuser pressures are shown normalized by test-section static pressure at the last calibration station in figure 12(a) and by sphere pressure in figure 12(b). The variation of sphere pressure with time is shown in figure 12(c). As indicated in the sketch at the top of figure 12(a), the diffuser has a two-dimensional ramp on the top and bottom of the axisymmetric diffuser. Since the measurements were made on the side of the diffuser, these ramps do not appreciably affect the flow until the shocks formed by the ramps intersect. This evidently occurs at $x_d/D \approx 3$. Disturbances upstream of the diffuser, such as shocks from the calibration rake and model support strut, cause the pressure to be relatively high at the diffuser entrance.

An expansion occurs in the sidewall static pressure until the effects of the ramps are felt, then the combined effects of shock interaction and wall boundary-layer growth force the static pressure to rise toward sphere pressure. It should be noted that the vacuum isolation valve is located at the end of the diffuser and that downstream of this valve are further sections of pipe, approximately 9.1 m (30 ft) long, which turn the diffuser flow approximately 150° and duct it into the spheres. Thus, further pressure recovery occurs downstream of the main diffuser section.

The pressure data for $x_d/D < 3$ shown normalized with respect to test-section static pressure in figure 12(a) indicate that the flow in this region is supersonic and not appreciably affected by back pressure, since the pressure level does not vary appreciably with time (for $t < 4$ sec). Downstream of this point, the pressure level usually increases significantly with time as well as distance, indicating that the increasing back (or sphere) pressure feeds upstream through the sidewall viscous flow and alters the flow pattern in the diffuser.

Static pressures in vicinity of vacuum isolation valve.- The use of unsymmetrical model mounting (unsymmetrical about a horizontal axis) and an unsymmetrical "butterfly" plate in the vacuum isolation valve introduce the possibility of unbalanced loading on the valve. If this loading is large enough, the valve could fail and block the tunnel, causing catastrophic failure of tunnel components due to overpressurization. A valve failure of

this type has occurred and this accounts for the present 1379 N/cm^2 (2000 psia) stagnation-pressure limitation on the tunnel. With the eventual installation of a gate valve, the facility can operate with a supply pressure of 2758 N/cm^2 (4000 psia).

During the present tests, static-pressure measurements were made in the vicinity of the valve at the locations indicated in figure 13, where the butterfly plate is shown in the open position. Because measurements of the actual pressures on the valve plate surface were not possible, the measurements on the walls at the indicated locations have been interpreted as indicating pressure levels affecting the valves.

Time histories of the pressure measurements upstream and downstream of the valve center line are shown in figure 13. These data indicate a region of fairly constant pressure up to $2\frac{1}{2}$ sec, even though the back pressure is building up. (See fig. 12(c).) After this period a wave system moving in the upstream direction evidently sweeps past the valve, and the pressure thereafter increases rapidly with time. The largest pressure change across the valve seems to occur at about $3\frac{1}{2}$ sec when the pressure difference across the front surface is small, but the pressure difference across the back surface is large. A typical combined pressure change across the valve butterfly plate is shown in figure 14. A positive value of Δp corresponds to a counterclockwise closing torque on the valve. The value shown corresponds to the pressure difference across orifices 12 and 13 added to the pressure difference across orifices 14 and 15. As expected from the discussion in connection with figure 13, the maximum torque occurs at $3\frac{1}{2}$ sec, and there is a rapid variation in sign of the torque across the valve when the moving wave system passes.

Measurements of the actual torsional vibration of the valve shaft indicated rms values of up to 0.08° with a frequency of about 40 Hz. A peak in the torsional vibration was observed to occur at the same time as the peak and rapid change in Δp indicated in figure 14. In addition, measurements were made of the instantaneous pressure at orifice 16 (see fig. 13) as a function of time using a small-volume pressure transducer. The observed signal recorded on an analog recorder indicated appreciable signal content at all frequencies up to the resolution of the recorder (about 400 Hz), and the magnitude of the peak-to-peak fluctuation was close to 100 percent of the mean level.

CONCLUDING REMARKS

Detailed flow characteristics in the Mach 20 leg of the Langley high Reynolds number helium tunnels have been determined for stagnation pressures from 207 to 1379 N/cm^2 (300 to 2000 psia) at ambient stagnation temperature. For this range of stagnation pres-

sure, the free-stream Mach number varies from 16.7 to 18.4, with a corresponding Reynolds number range from 7.6×10^6 to 48.6×10^6 per meter (2.3×10^6 to 14.8×10^6 per ft). The axial Mach number gradient has been found to be 0.125 per meter (0.038 per ft) and the inviscid core approximately 50.8 cm (20 in.) in diameter. Nondimensional radial distributions of Mach numbers are similar to distributions obtained previously in the Langley 22-inch helium tunnel. Pressures measured along the sidewall of the diffuser demonstrate the change in flow conditions within the diffuser as back pressure rises during the run. Also, measured maximum peaks in valve-shaft deflection on a 183-cm-diameter (72-in.) butterfly valve downstream of the diffuser are correlated with peaks in pressure loading measured at the valve.

Langley Research Center,
National Aeronautics and Space Administration,
Hampton, Va., August 31, 1971.

REFERENCES

1. Bogdonoff, S. M.; and Hammitt, A. G.: The Princeton Helium Hypersonic Tunnel and Preliminary Results Above M = 11. WADC Tech. Rep. 54-124, U.S. Air Force, July 1954.

2. Witcofski, Robert D.; and Henderson, Arthur, Jr.: Induced Pressures on Cylindrical Rods With Various Nose Drags and Nose Shapes at Mach Numbers of 17 and 21. NASA TN D-1266, 1962.

3. Kemp, Joseph H., Jr.: The Ames M-50 Helium Tunnel. NASA TN D-5788, 1970.

4. Erickson, Wayne D.: An Extension of Estimated Hypersonic Flow Parameters for Helium as a Real Gas. NASA TN D-1632, 1963.

5. Morkovin, Mark V.: Signal Interpretation in High-Speed Anemometry – A Review. Advances in Hot-Wire Anemometry, W. L. Melnik and J. R. Weske, eds., AFOSR No. 68-1492, U.S. Air Force, July 1968, pp. 38-51. (Available from DDC as AD 676 019.)

6. Weinstein, Leonard M.; Wagner, Richard D., Jr.; Henderson, Arthur, Jr.; and Ocheltree, Stewart L.: Electron Beam Flow Visualization in Hypersonic Helium Flow. ICIASF '69 Record, IEEE Publ. 69-C-69 AES, pp. 72-78.

7. Johnson, Charles B.; Boney, Lillian R.; Ellison, James C.; and Erickson, Wayne D.: Real-Gas Effects on Hypersonic Nozzle Contours With a Method of Calculation. NASA TN D-1622, 1963.

8. Persh, Jerome; and Lee, Roland: A Method for Calculating Turbulent Boundary Layer Development in Supersonic and Hypersonic Nozzles Including the Effects of Heat Transfer. NAVORD Rep. 4200 (Aeroballistic Res. Rep. 320), U.S. Navy, June 7, 1956.

9. Kenney, James T.; and Yu, Ying-Nien: On the Length of Hypersonic Nozzles. J. Aero/Space Sci., vol. 25, no. 11, Nov. 1958, p. 724.

10. Fischer, Michael C.; Maddalon, Dal V.; Weinstein, Leonard M.; and Wagner, Richard D., Jr.: Boundary-Layer Surveys on a Nozzle Wall at $M_\infty \approx 20$ Including Hot-Wire Fluctuation Measurements. AIAA Paper No. 70-746, June-July 1970.

11. Mueller, James N.: Equations, Tables, and Figures for Use in the Analysis of Helium Flow at Supersonic and Hypersonic Speeds. NACA TN 4063, 1957.

12. Erickson, Wayne D.: Real-Gas Correction Factors for Hypersonic Flow Parameters in Helium. NASA TN D-462, 1960.

13. Maddalon, Dal V.; and Jackson, Willis E.: A Survey of the Transport Properties of Helium at High Mach Number Wind-Tunnel Conditions. NASA TM X-2020, 1970.

14. Clark, Frank L.; Ellison, James C.; and Johnson, Charles B.: Recent Work in Flow Evaluation and Techniques of Operations for the Langley Hypersonic Nitrogen Facility. Vol. I of Fifth Hypersonic Velocity Techniques Symposium, Univ. of Denver, Mar. 1967, pp. 347-373. (Available from DDC as AD 819715.)

TABLE I.- CAPABILITIES OF THE MACH 20 LEG OF THE LANGLEY HIGH REYNOLDS NUMBER HELIUM TUNNELS

[Quantities corrected for high-pressure real-gas effects and low-temperature quantum effects]

Quantity	Value at stagnation pressure of –					
	69 N/cm^2	(100 psi)	1379 N/cm^2	(2000 psi)	2758 N/cm^2 [a]	(4000 psi)
Average Mach number		16.3		18.4		19
Free-stream Reynolds number per m (per ft)	2.7×10^6	(0.81×10^6)	48.6×10^6	(14.8×10^6)	96.4×10^6	(29.4×10^6)
Free-stream pressure, N/cm^2 (psia)	0.09×10^{-2}	(0.13×10^{-2})	1.05×10^{-2}	(1.5×10^{-2})	1.92×10^{-2}	(2.8×10^{-2})
Dynamic pressure, N/cm^2 (psia)	0.20	(0.29)	2.97	(4.3)	5.78	(8.4)
Mass flow rate, kg/sec (lbm/sec)	1.36	(3.0)	28.4	(62.7)	60.1	(132.4)
Core size (approximate), cm (in.)	50.8	(20)	50.8	(20)	50.8	(20)
Test-section diameter, cm (in.)	152.4	(60)	152.4	(60)	152.4	(60)
Stagnation temperature, °K (°R)	300	(540)	300	(540)	300	(540)
Free-stream temperature, °K (°R)	3.3	(6.0)	2.7	(4.9)	2.6	(4.7)
Free-stream velocity, m/sec (ft/sec)	1758	(5768)	1787	(5863)	1813	(5947)
Run time, sec		6		6		6
Free-stream rms mass-flow fluctuations,[b] percent of mean		2.7		2.2		1.7

[a] Extrapolated from calibration data.

[b] Hot-wire measurements made by Richard D. Wagner, Jr., Langley Research Center.

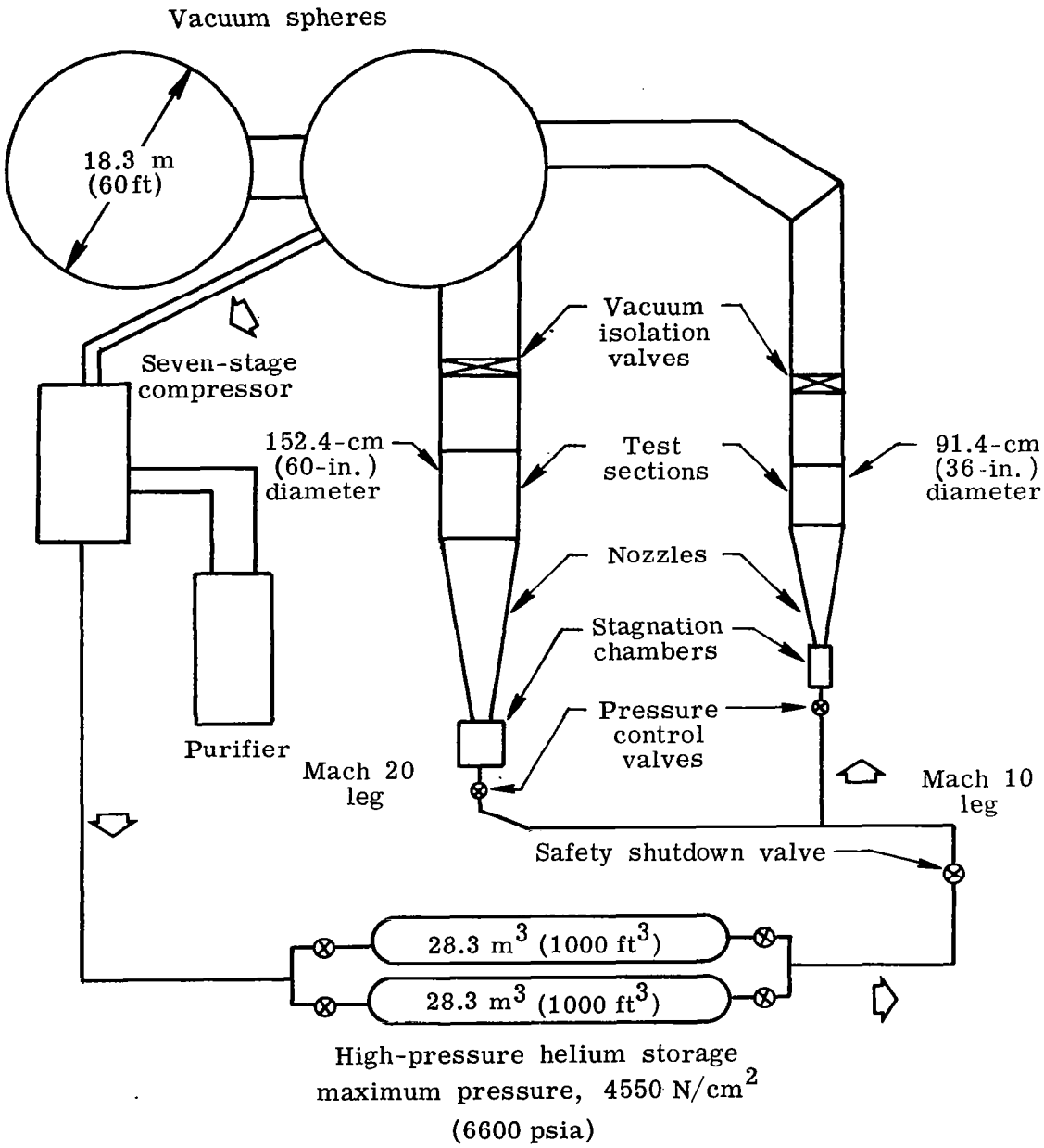

Figure 1.- Schematic of the Langley high Reynolds number helium tunnels.

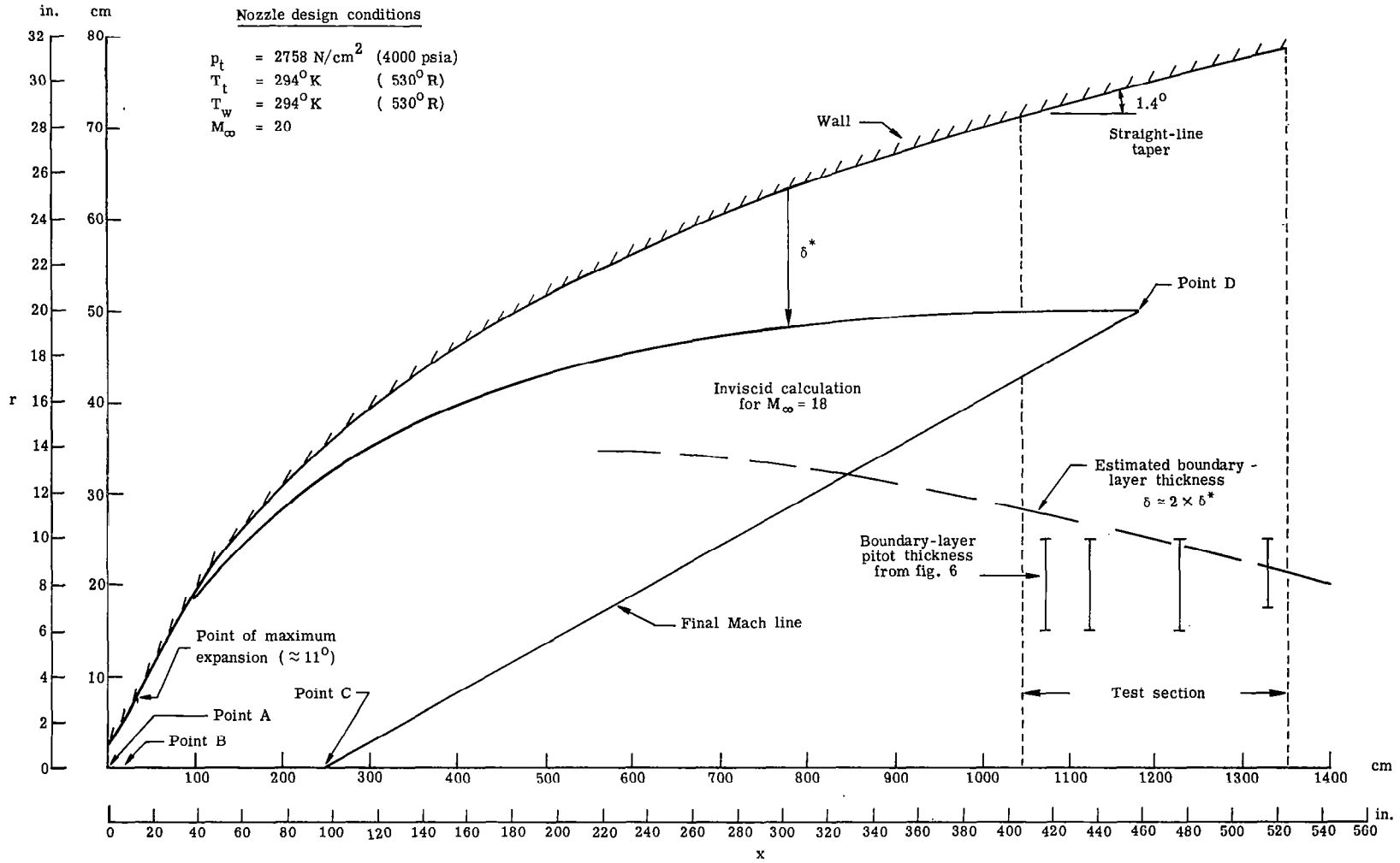

(a) Nozzle dimensions.

Figure 2.- Dimensions of the Mach 20 leg of the Langley high Reynolds number helium tunnels.

Throat diameter, d 5.1 (2.0)
Test-section diameter, D 152.4 (60)

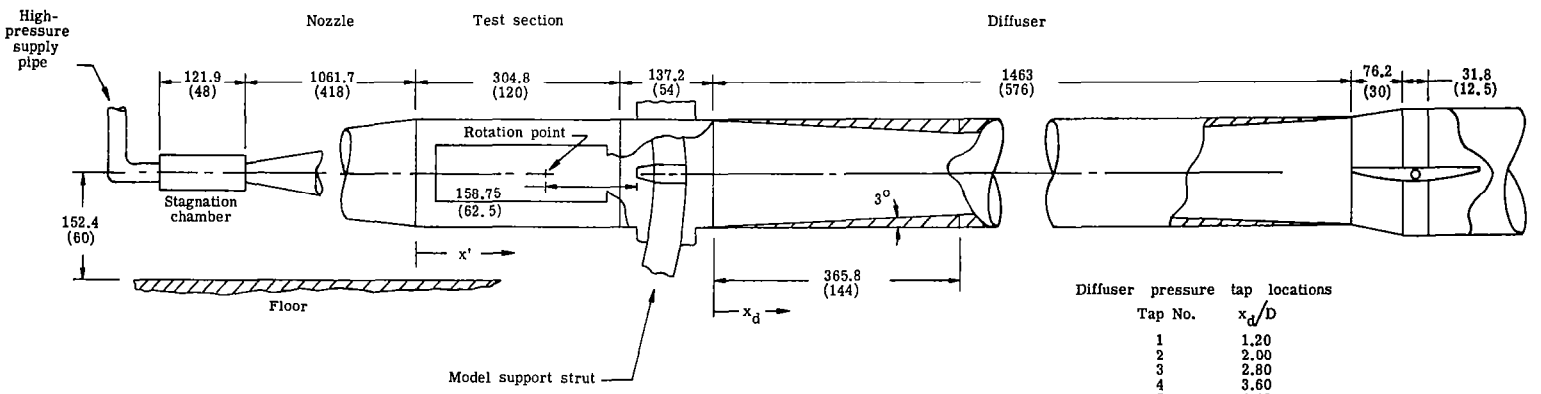

Diffuser pressure tap locations

Tap No.	x_d/D
1	1.20
2	2.00
3	2.80
4	3.60
5	4.40
6	5.20
7	6.00
8	6.80
9	7.60
10	8.40
11	9.20

(b) Overall tunnel dimensions in cm and (in.).

Figure 2.- Concluded.

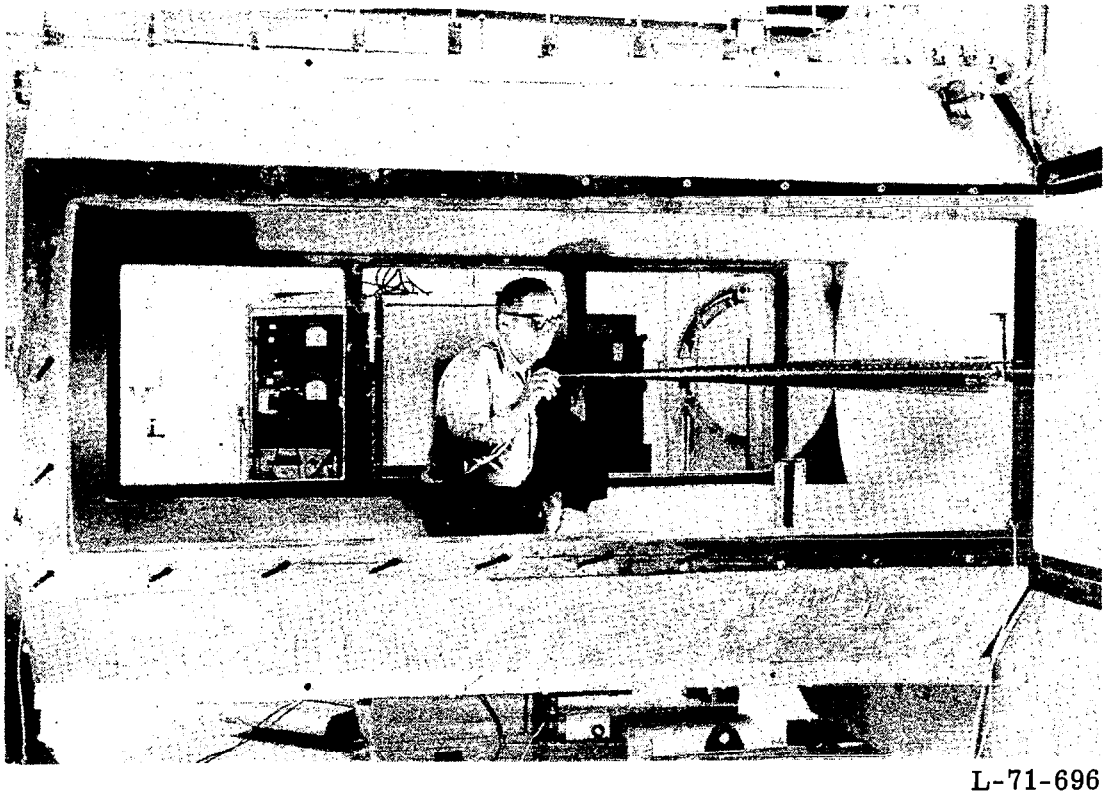

L-71-696

Figure 3.- Photograph of Mach 20 test section.

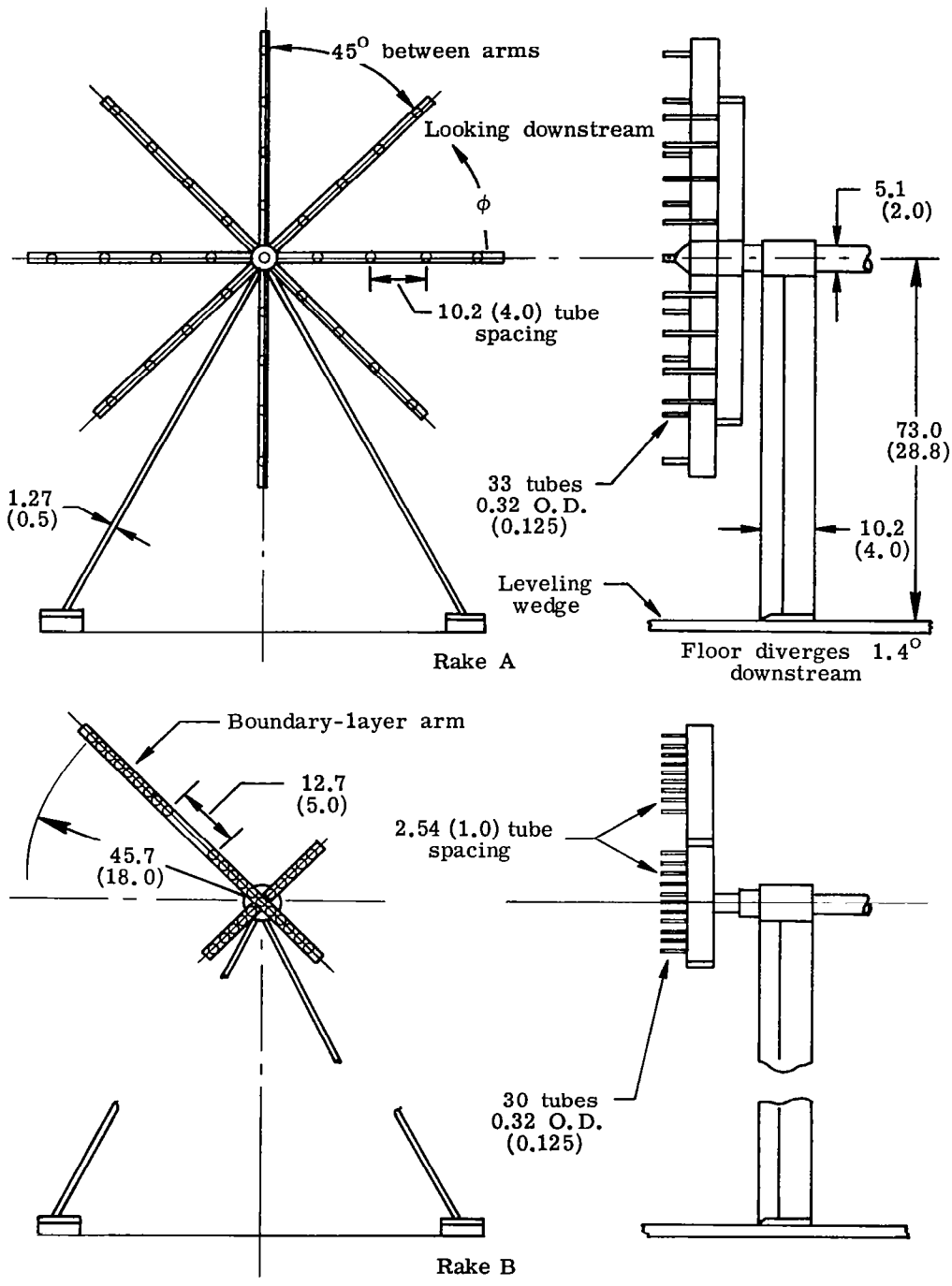

Figure 4.- Rake dimensions in cm and (in.).

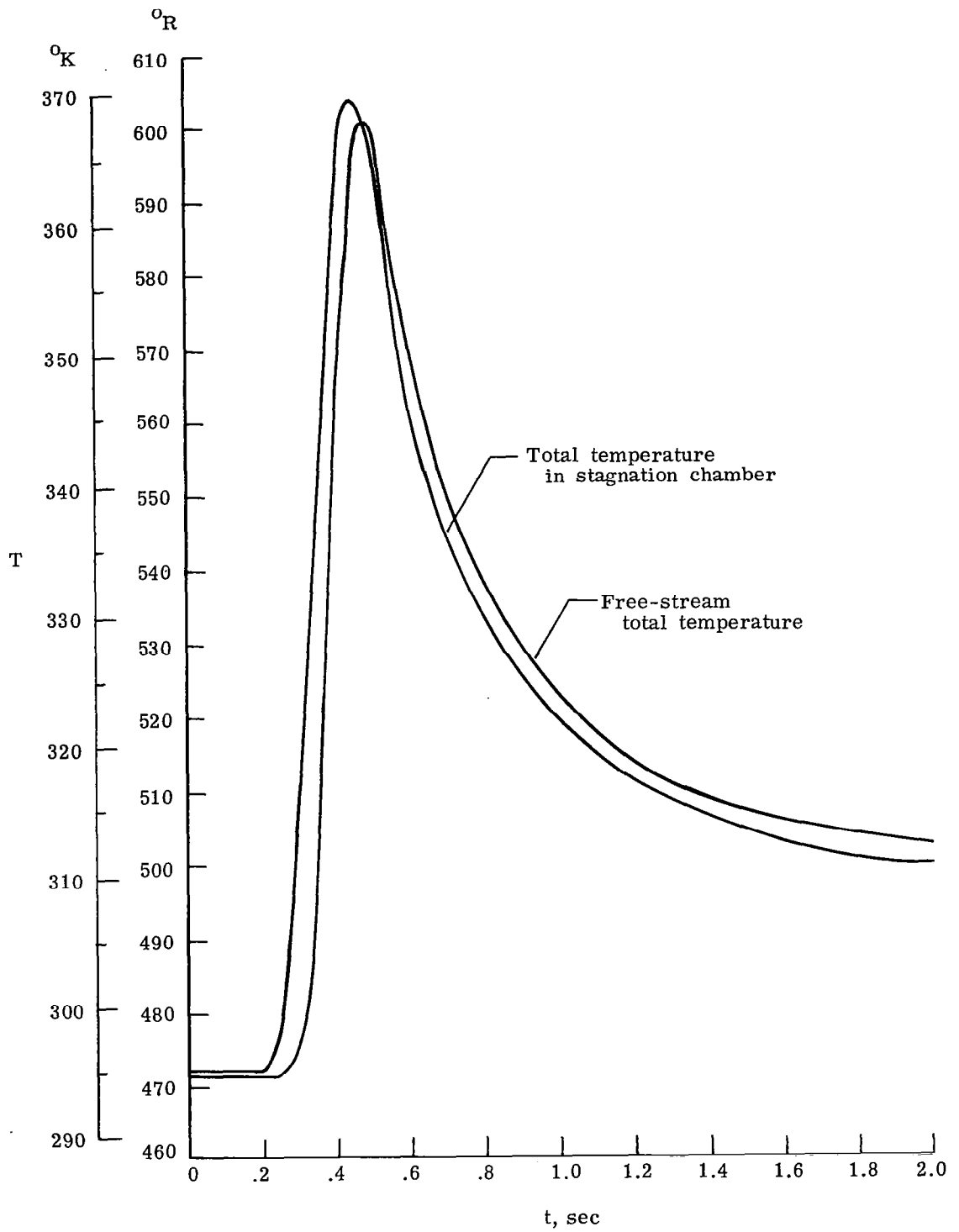

Figure 5.- Typical total temperature value during tunnel start.
p_t = 345 N/cm^2 (500 psia).

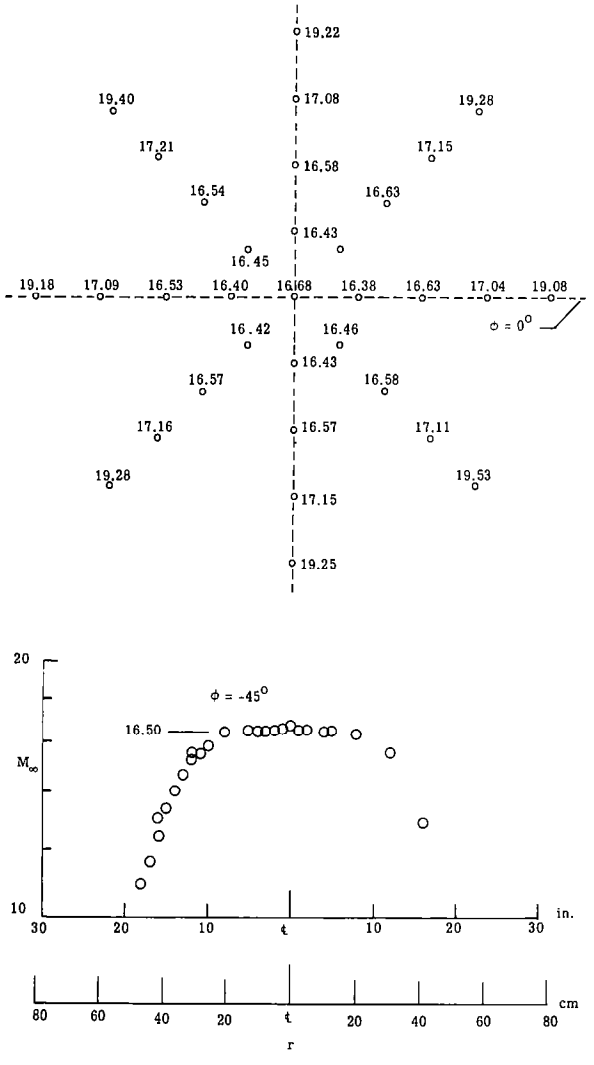

(a) Station 1. p_t = 207 N/cm^2 (300 psia); T_t = 308° K (555° R).

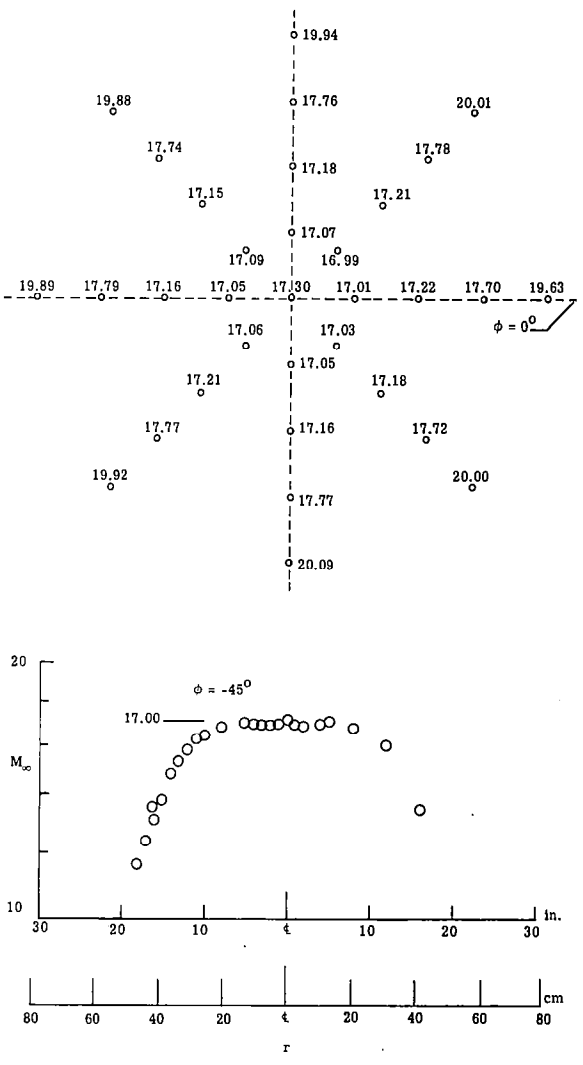

(b) Station 1. p_t = 346 N/cm^2 (502 psia); T_t = 305° K (549° R).

Figure 6.- Mach number distribution in test section. (In upper part of figure, M is determined from ratio of pitot to stagnation pressure. In lower part, for r > 5, M is determined from ratio of pitot to static pressure.)

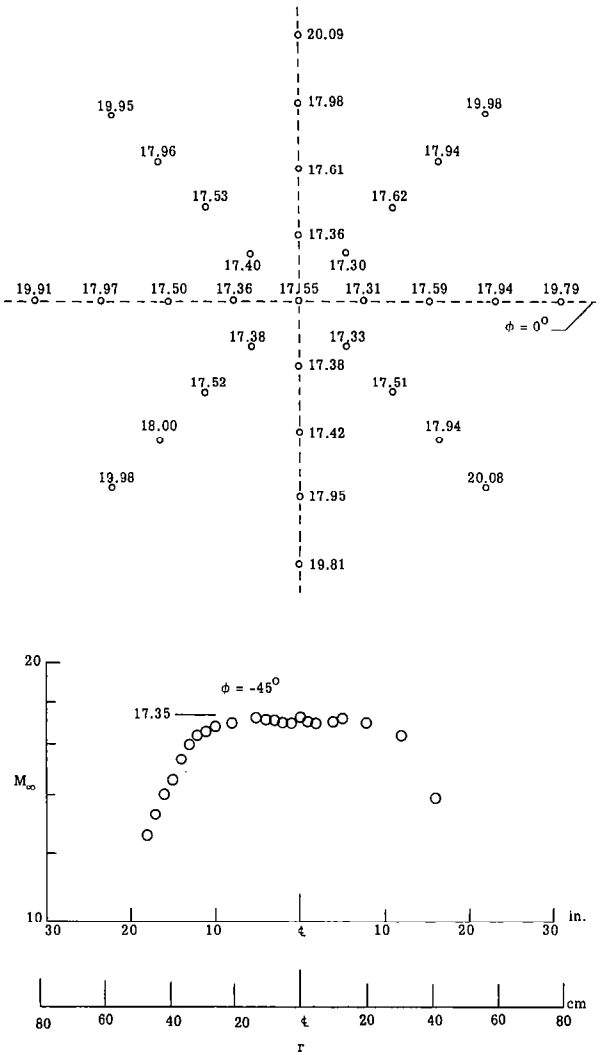

(c) Station 1. $p_t = 483$ N/cm^2 (701 psia); $T_t = 301^o$ K (542^o R).

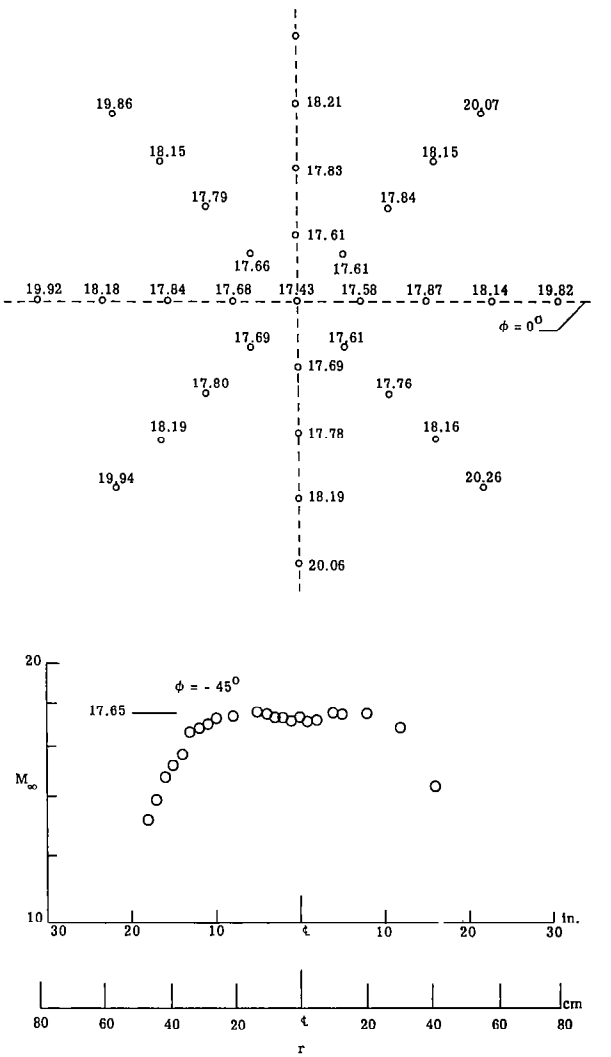

(d) Station 1. $p_t = 672$ N/cm^2 (974 psia); $T_t = 295^o$ K (531^o R).

Figure 6.- Continued.

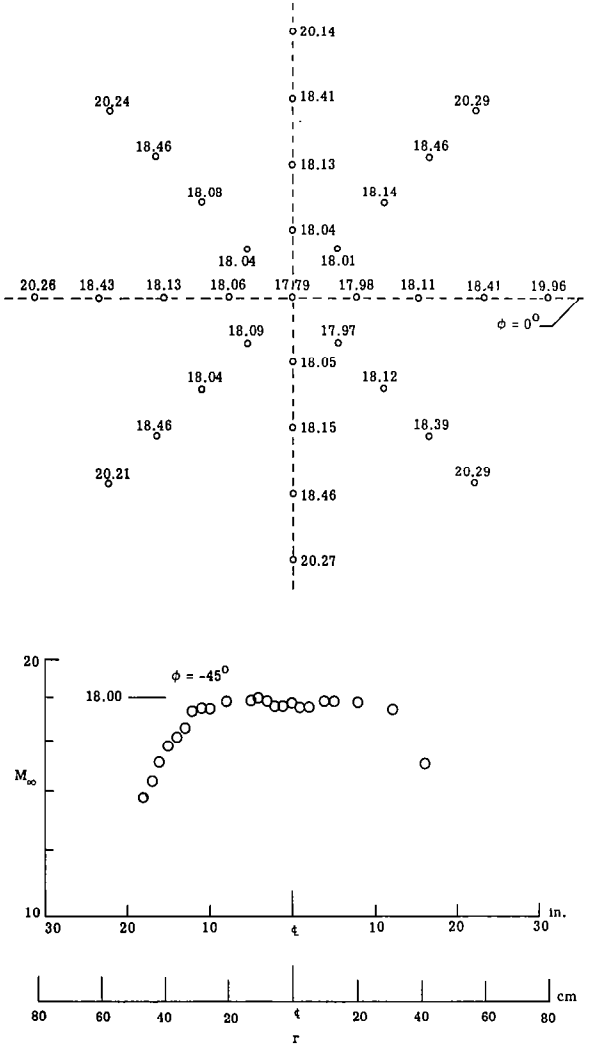

(e) Station 1. p_t = 1007 N/cm^2 (1460 psia); T_t = 309° K (556° R).

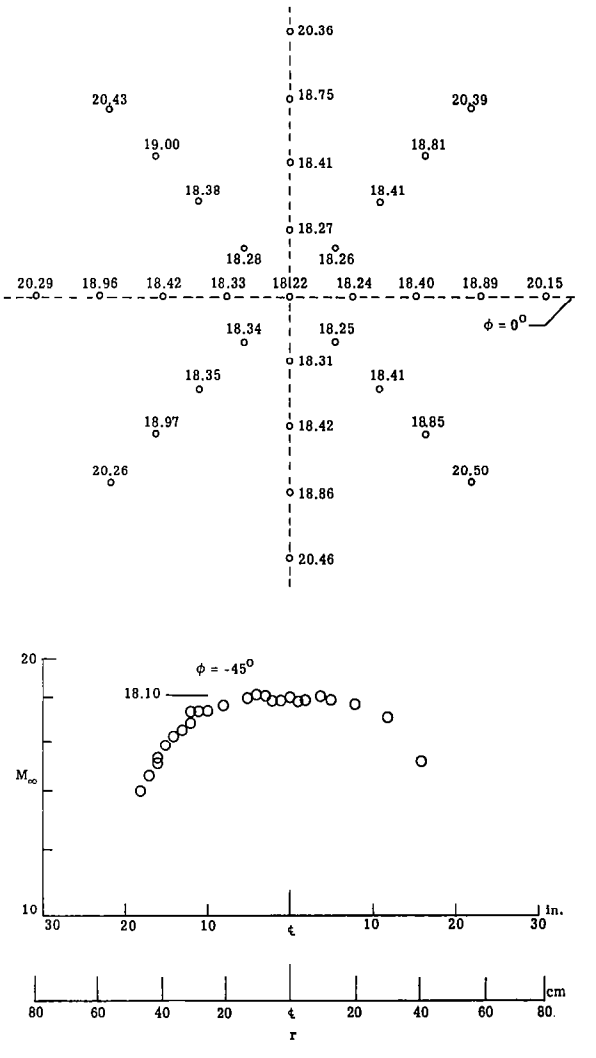

(f) Station 1. p_t = 1343 N/cm^2 (1948 psia); T_t = 300° K (540° R).

Figure 6.- Continued.

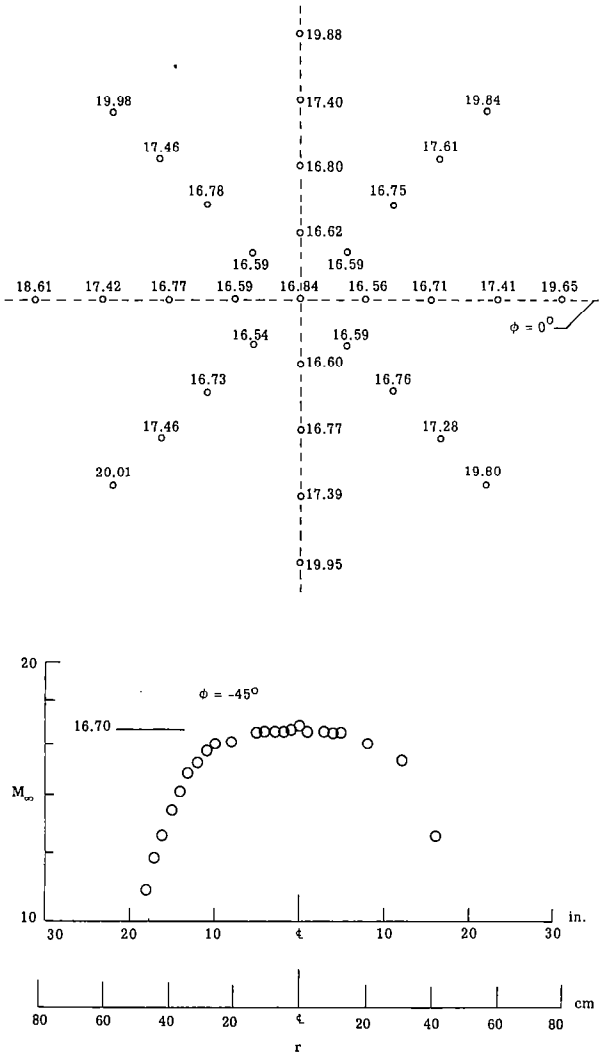

(g) Station 2. p_t = 191 N/cm^2 (277 psia); T_t = 307° K (552° R).

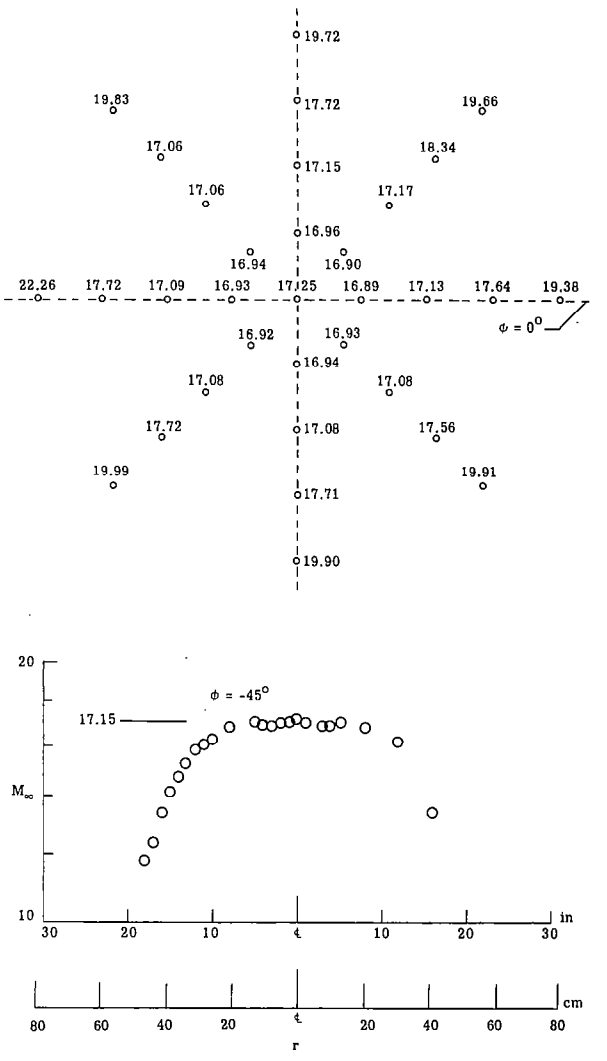

(h) Station 2. p_t = 323 N/cm^2 (469 psia); T_t = 303° K (545° R).

Figure 6.- Continued.

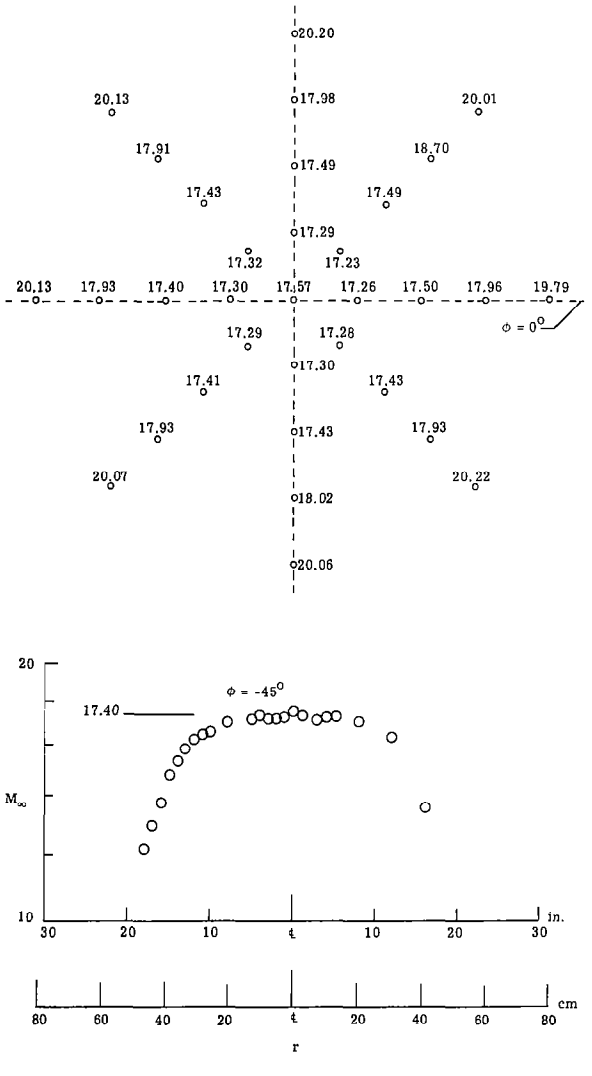

(i) Station 2. p_t = 469 N/cm^2 (680 psia); T_t = 307° K (552° R).

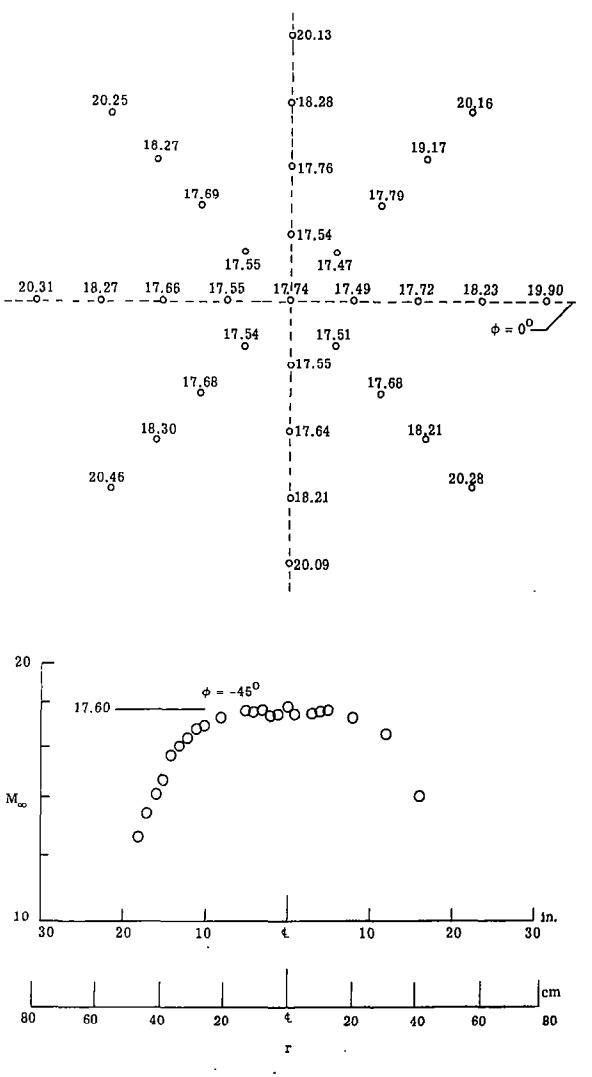

(j) Station 2. p_t = 662 N/cm^2 (960 psia); T_t = 299° K (538° R).

Figure 6.- Continued.

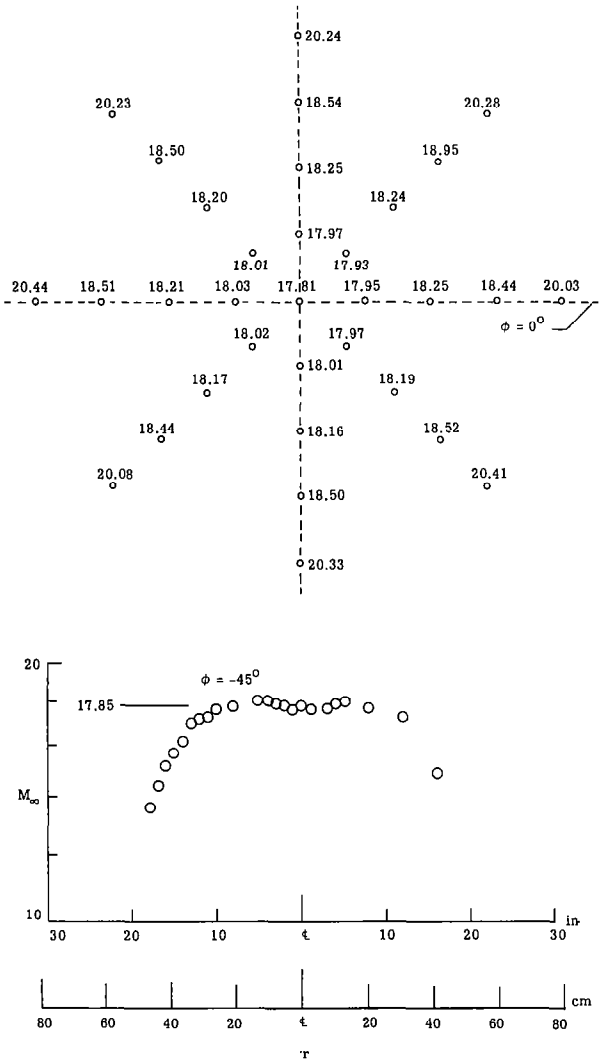

(k) Station 2. p_t = 1011 N/cm^2 (1466 psia); T_t = 294^o K (530^o R).

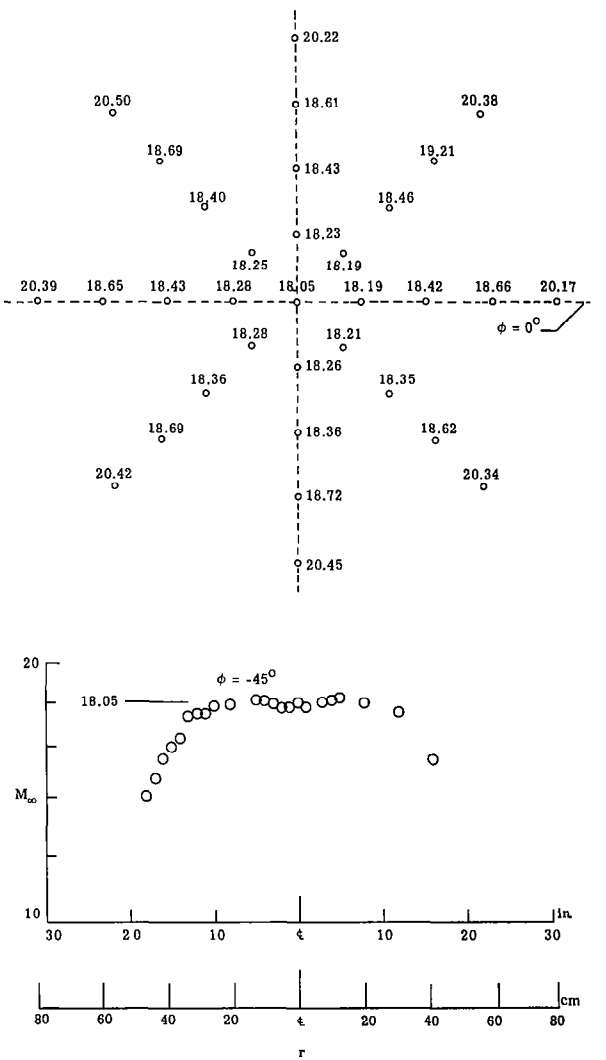

(l) Station 2. p_t = 1217 N/cm^2 (1765 psia); T_t = 297^o K (535^o R).

Figure 6.- Continued.

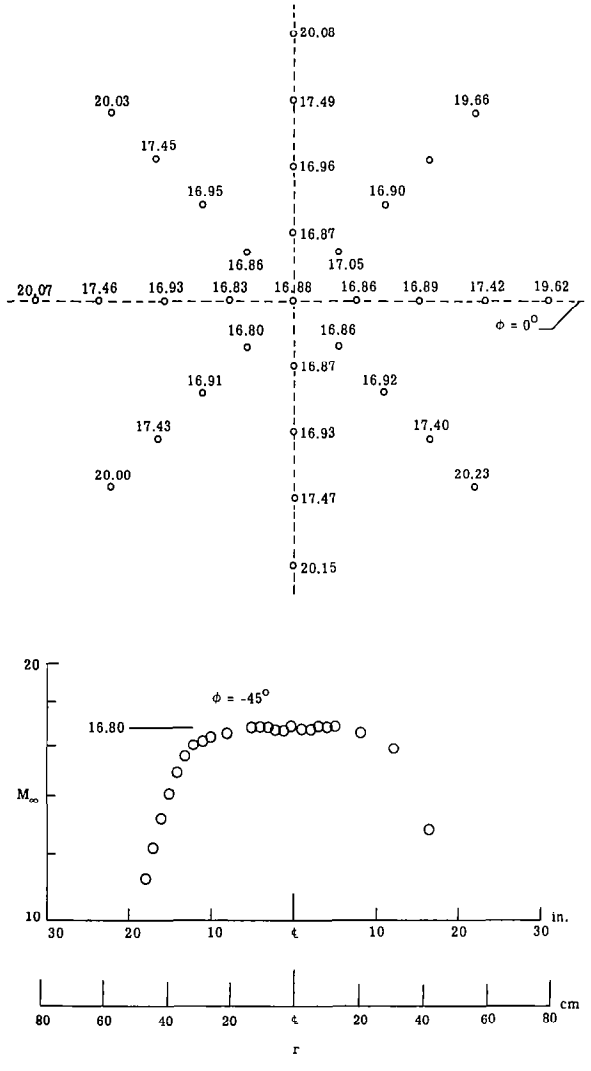

(m) Station 3. p_t = 203 N/cm^2 (295 psia); T_t = 302^o K (544^o R).

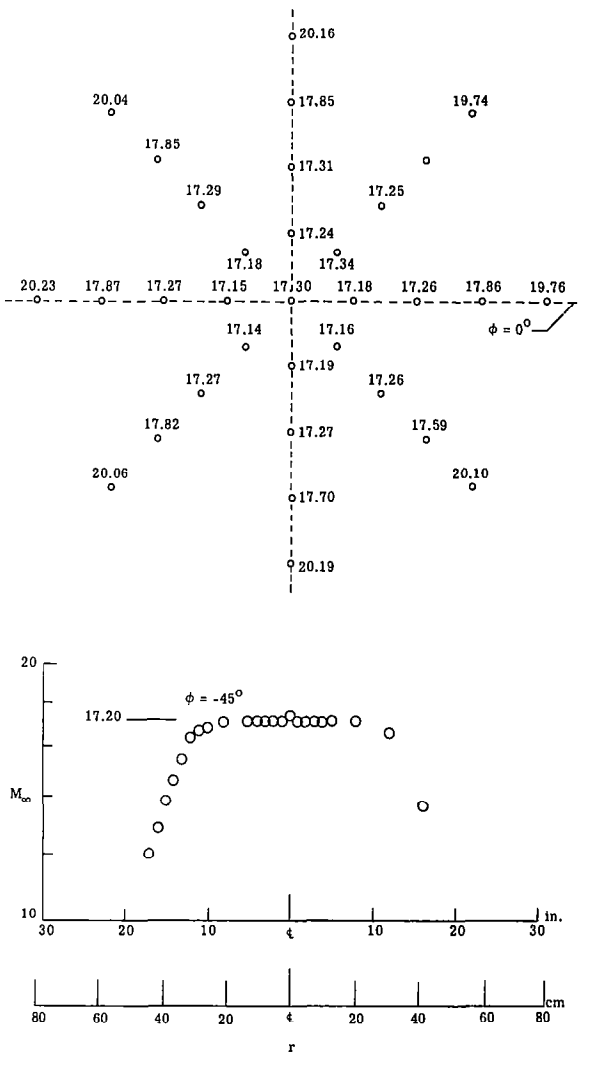

(n) Station 3. p_t = 339 N/cm^2 (492 psia); T_t = 301^o K (542^o R).

Figure 6.- Continued.

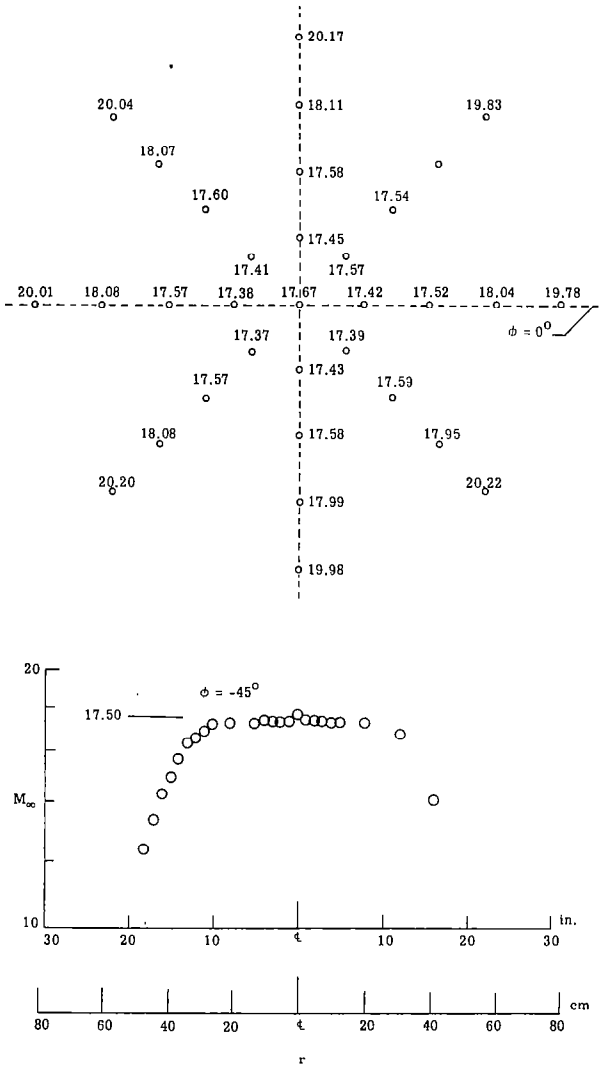

(o) Station 3. p_t = 479 N/cm^2 (694 psia); T_t = 302^o K (543^o R).

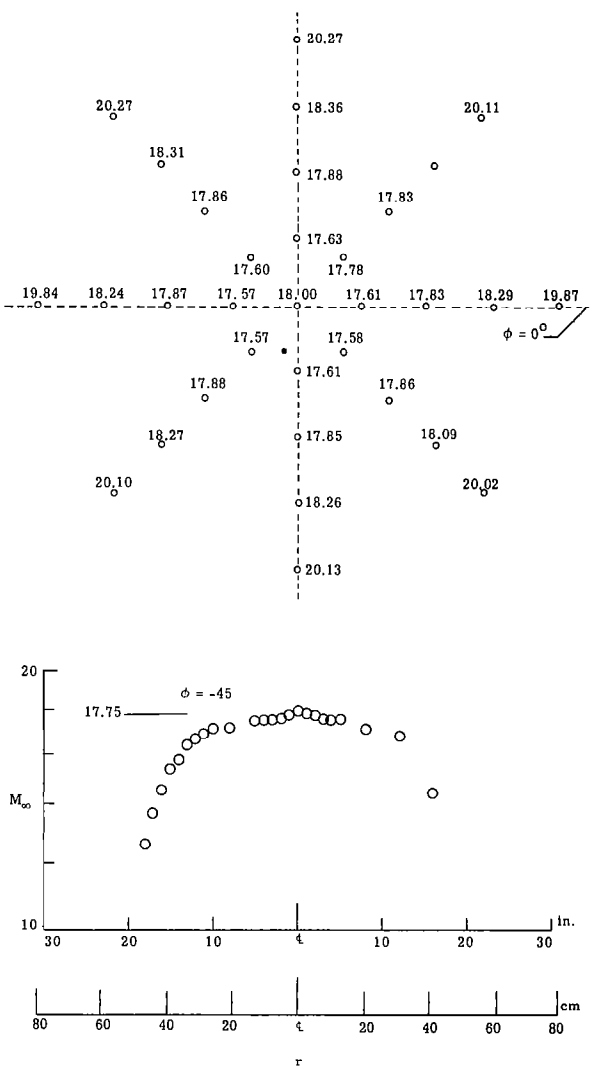

(p) Station 3. p_t = 661 N/cm^2 (958 psia); T_t = 299^o K (538^o R).

Figure 6.- Continued.

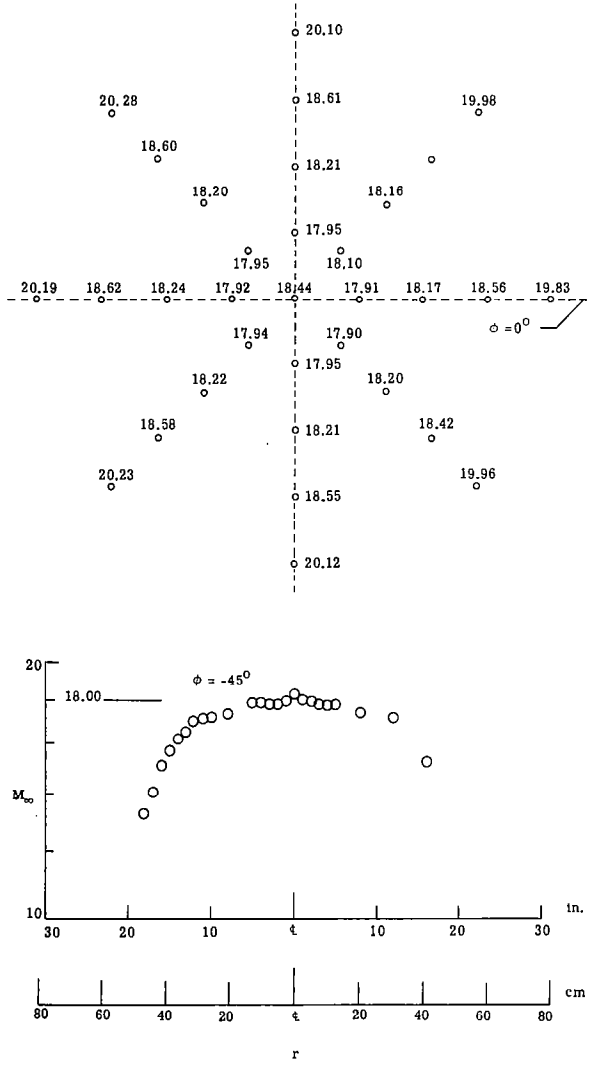

(q) Station 3. p_t = 995 N/cm^2 (1443 psia); T_t = 294^0 K (530^0 R).

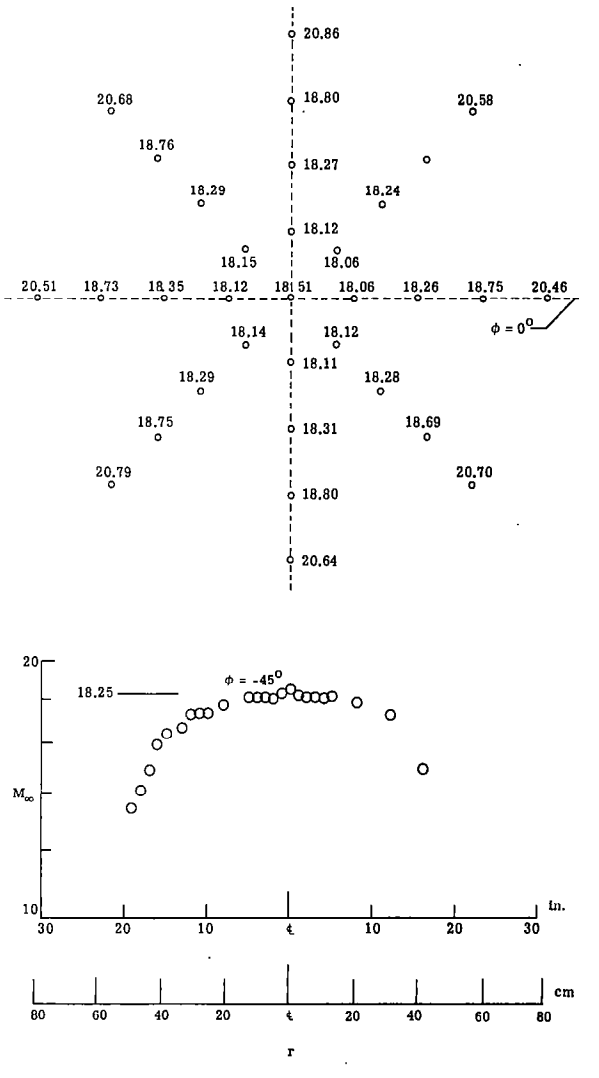

(r) Station 3. p_t = 1325 N/cm^2 (1922 psia); T_t = 297^0 K (535^0 R).

Figure 6.- Continued.

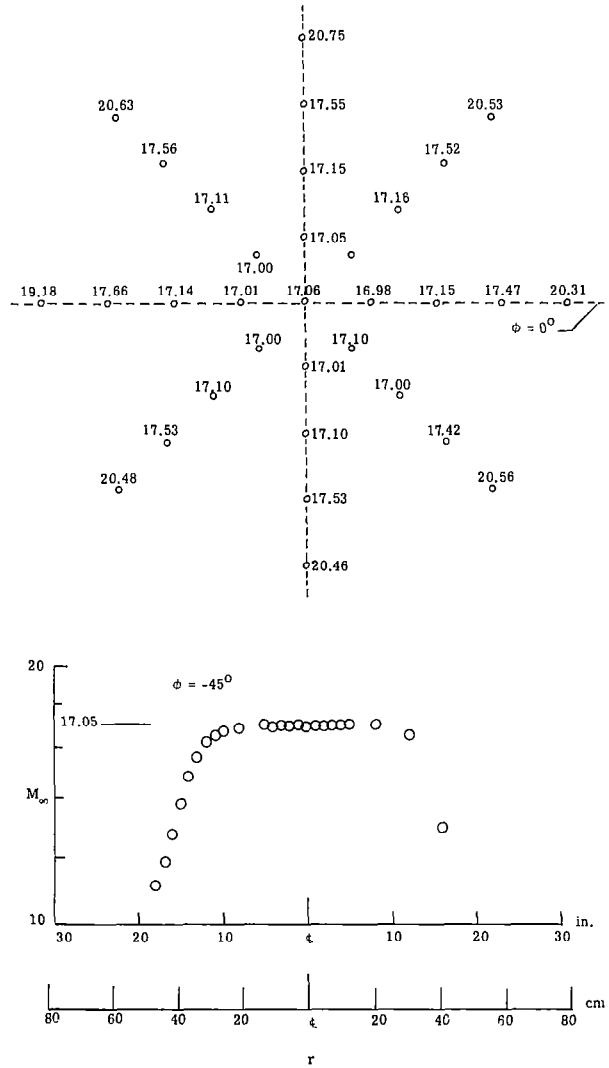

(s) Station 4. p_t = 195 N/cm^2 (283 psia); T_t = 311^o K (560^o R).

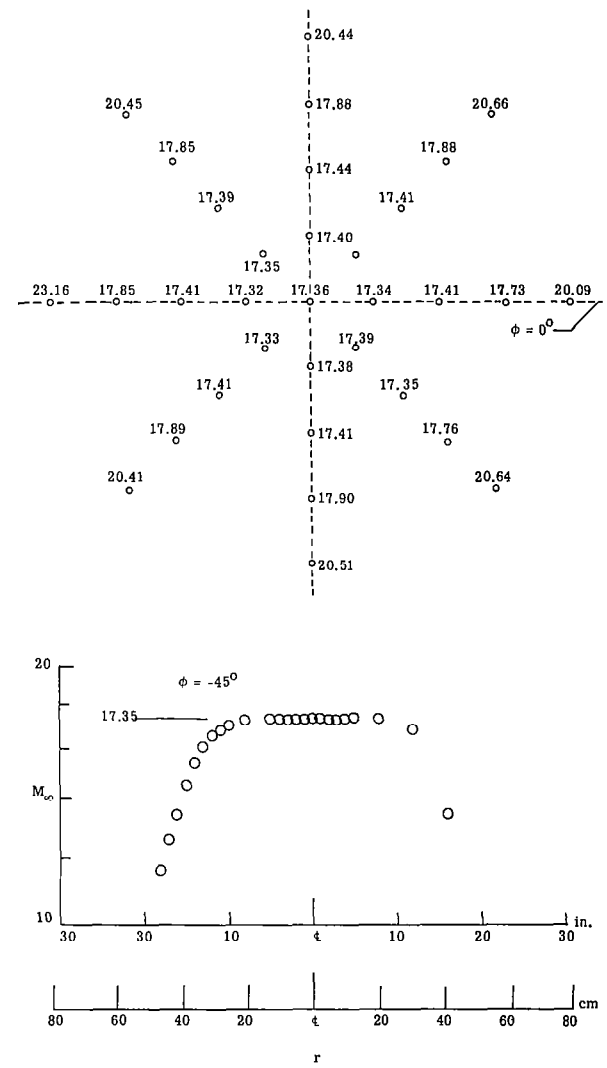

(t) Station 4. p_t = 343 N/cm^2 (498 psia); T_t = 308^o K (554^o R).

Figure 6.- Continued.

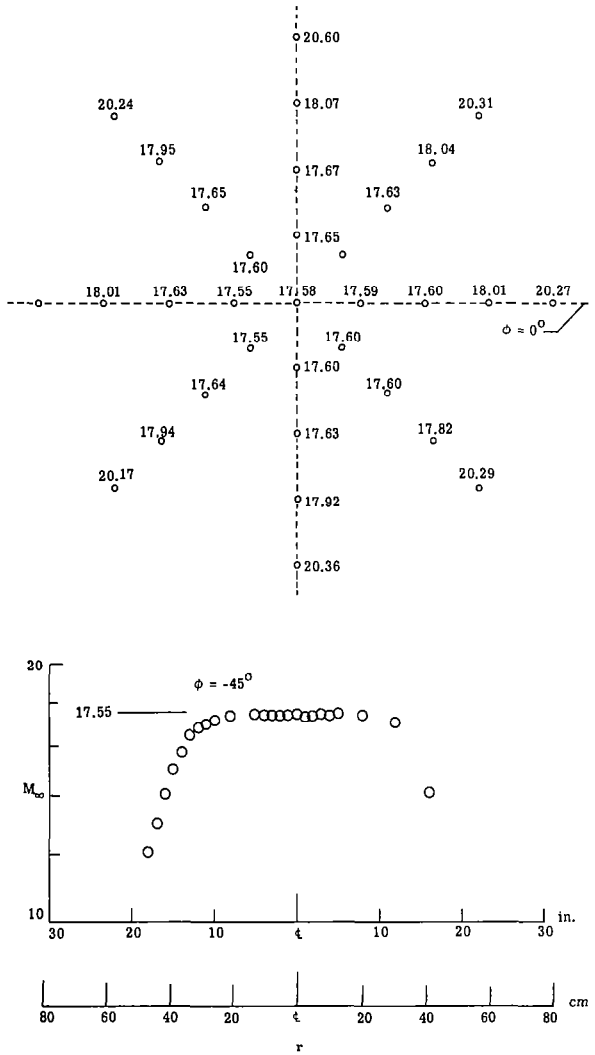

(u) Station 4. p_t = 480 N/cm^2 (696 psia); T_t = 305^o K (550^o R).

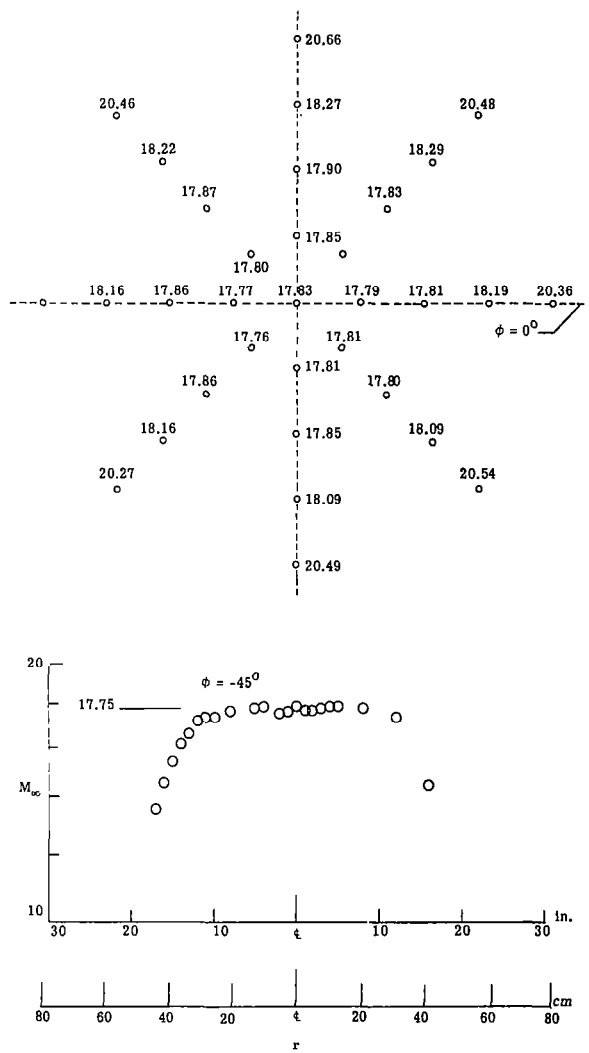

(v) Station 4. p_t = 667 N/cm^2 (967 psia); T_t = 304^o K (547^o R).

Figure 6.- Continued.

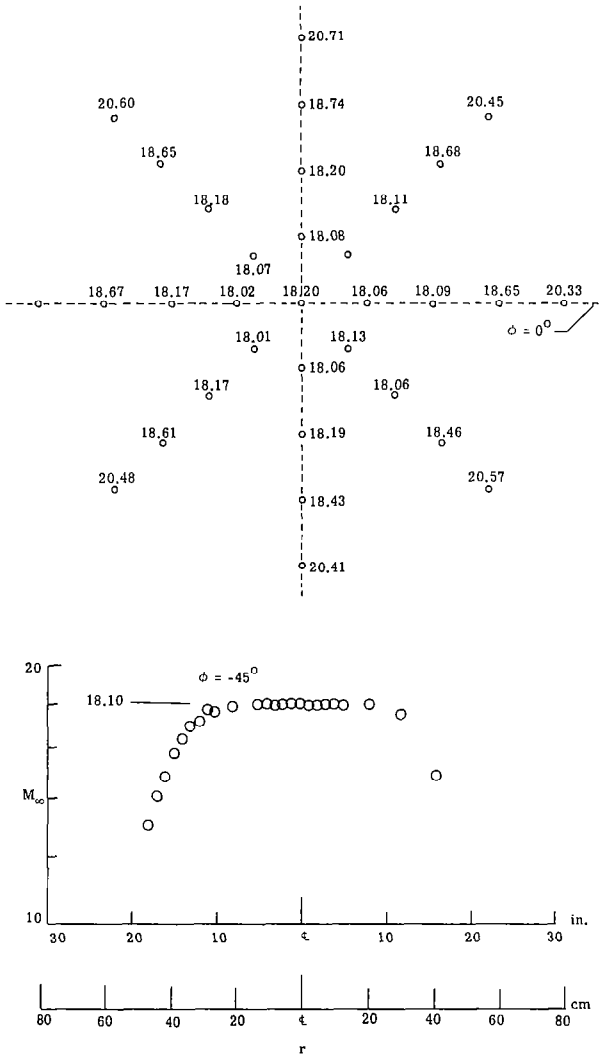

(w) Station 4. p_t = 1011 N/cm^2 (1466 psia); T_t = 300° K (541° R).

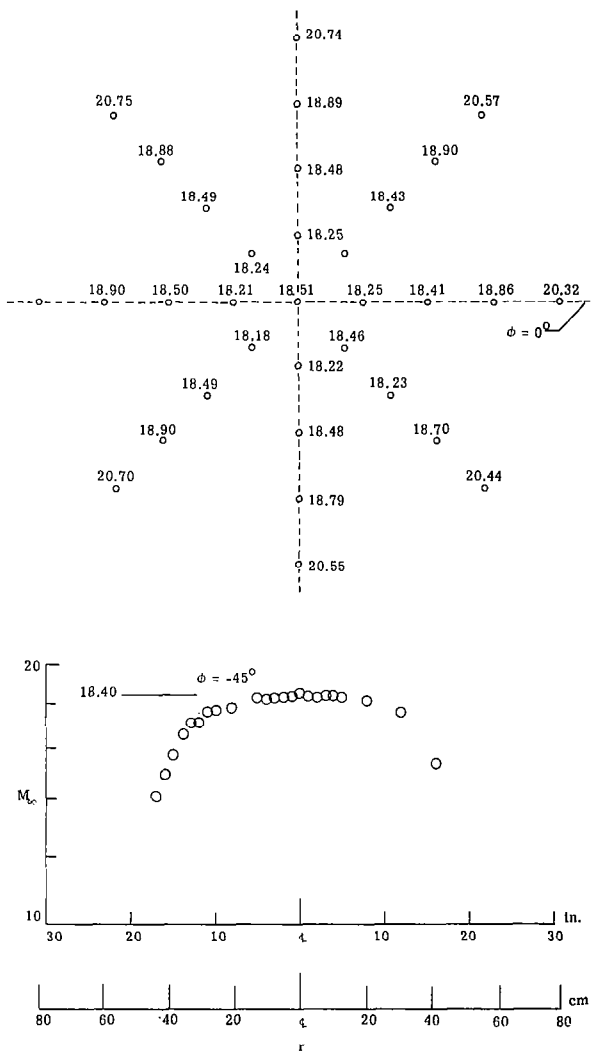

(x) Station 4. p_t = 1336 N/cm^2 (1937 psia); T_t = 303° K (545° R).

Figure 6.- Concluded.

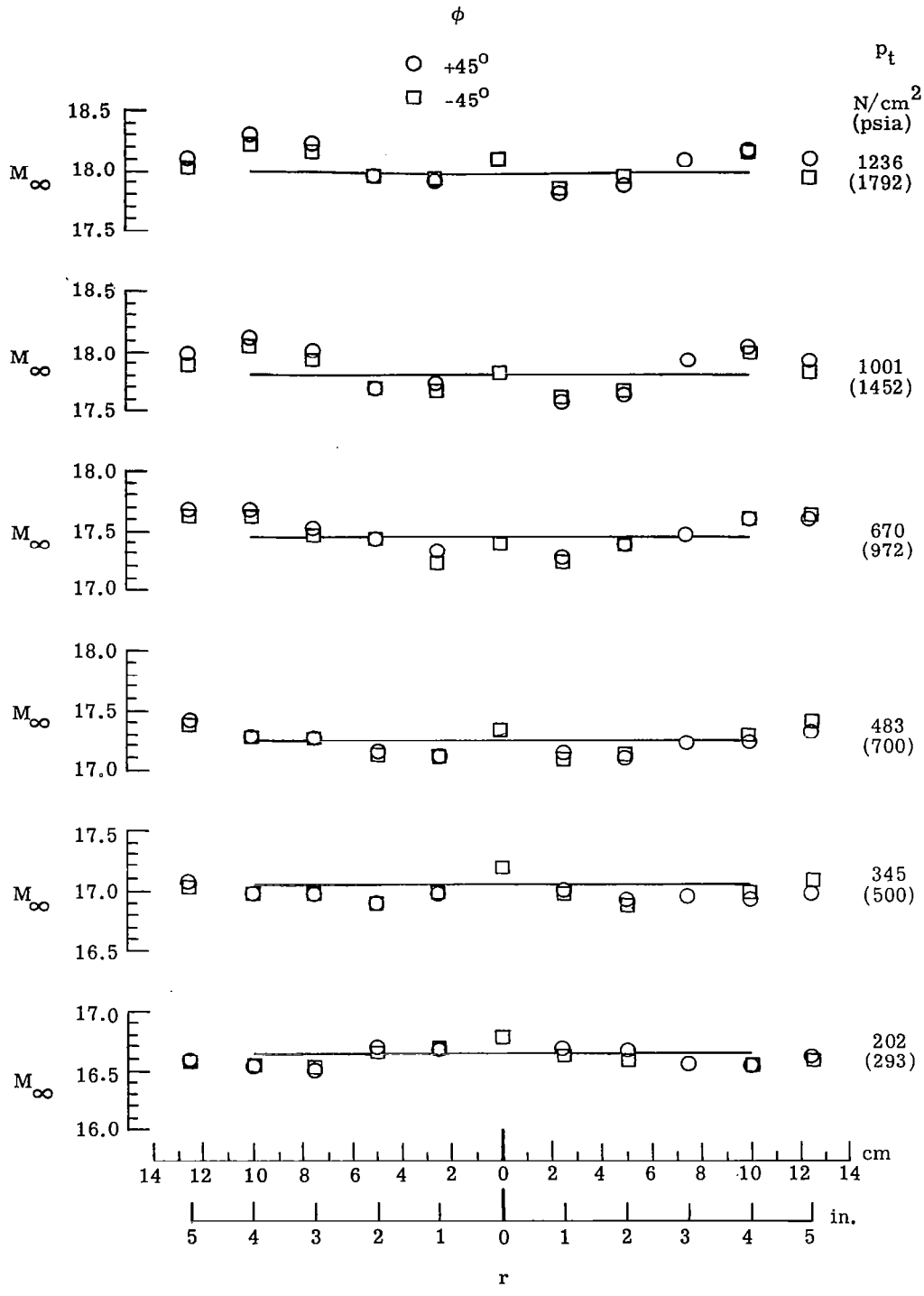

(a) Station 1. x' = 30.15 cm (11.87 in.).

Figure 7.- Mach number distributions in 25.4-cm-diameter (10-in.) core.

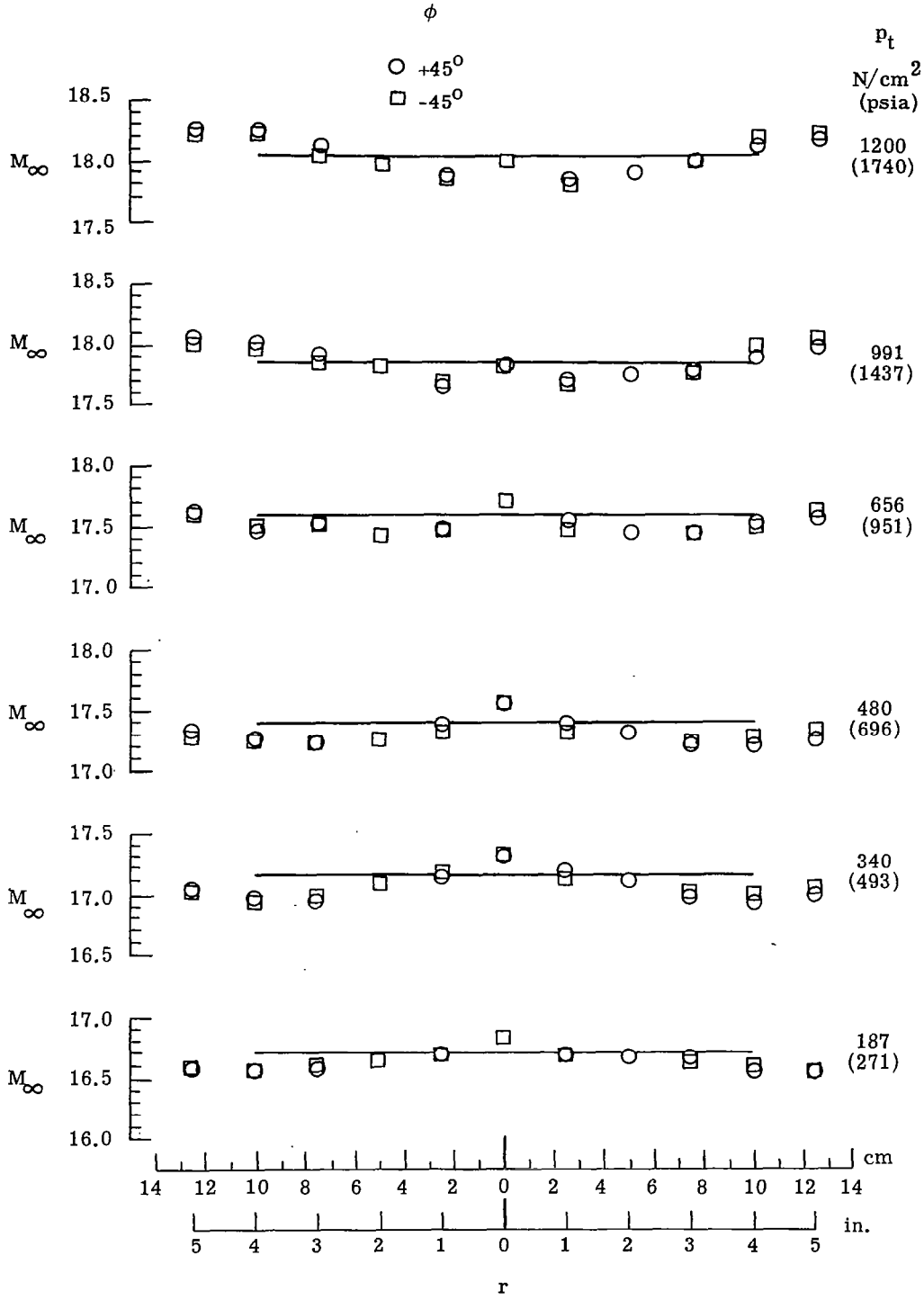

(b) Station 2. x' = 80.95 cm (31.87 in.).

Figure 7.- Continued.

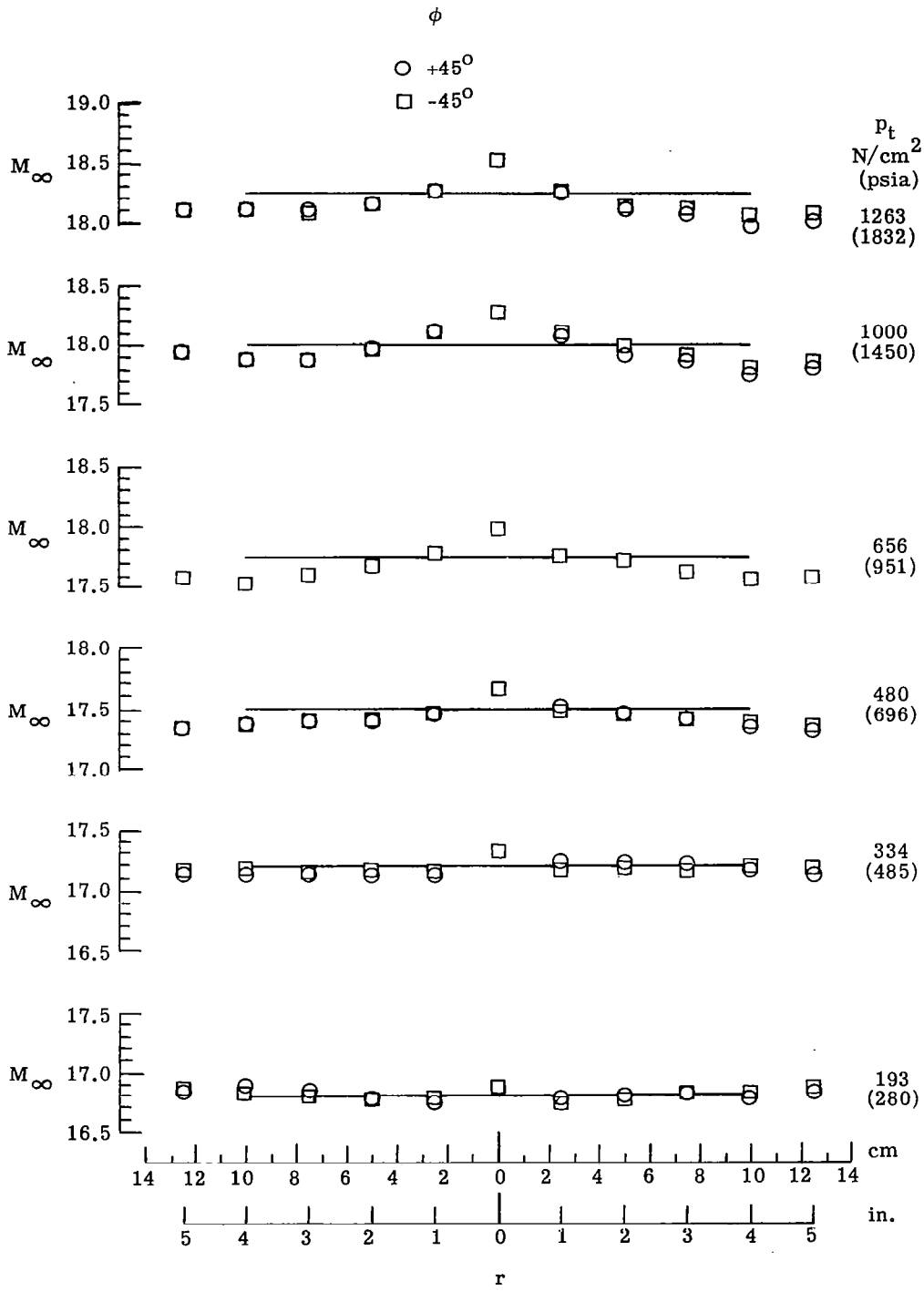

(c) Station 3. x' = 182.5 cm (71.85 in.).

Figure 7.- Continued.

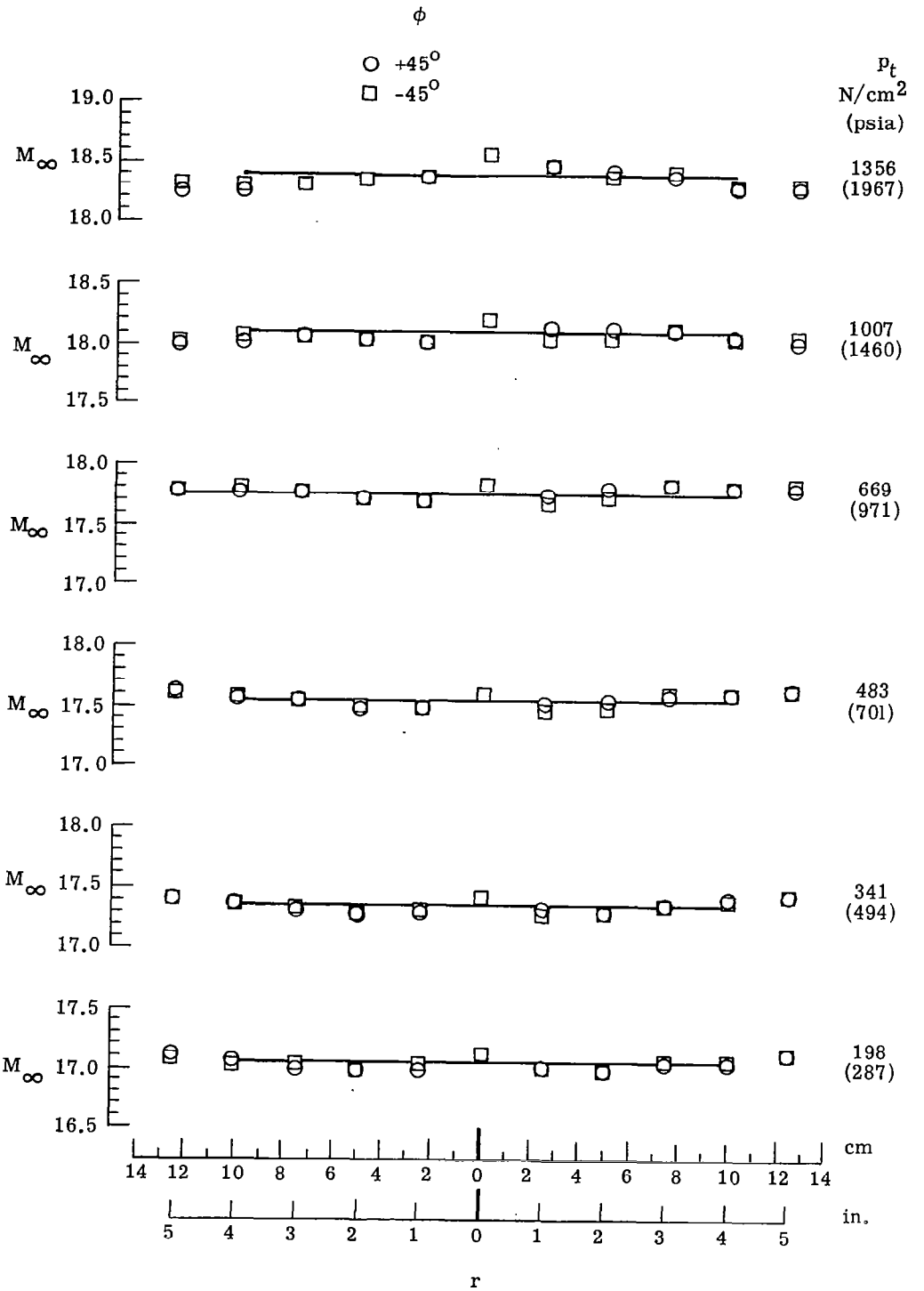

(d) Station 4. x' = 284.1 cm (111.85 in.).

Figure 7.- Concluded.

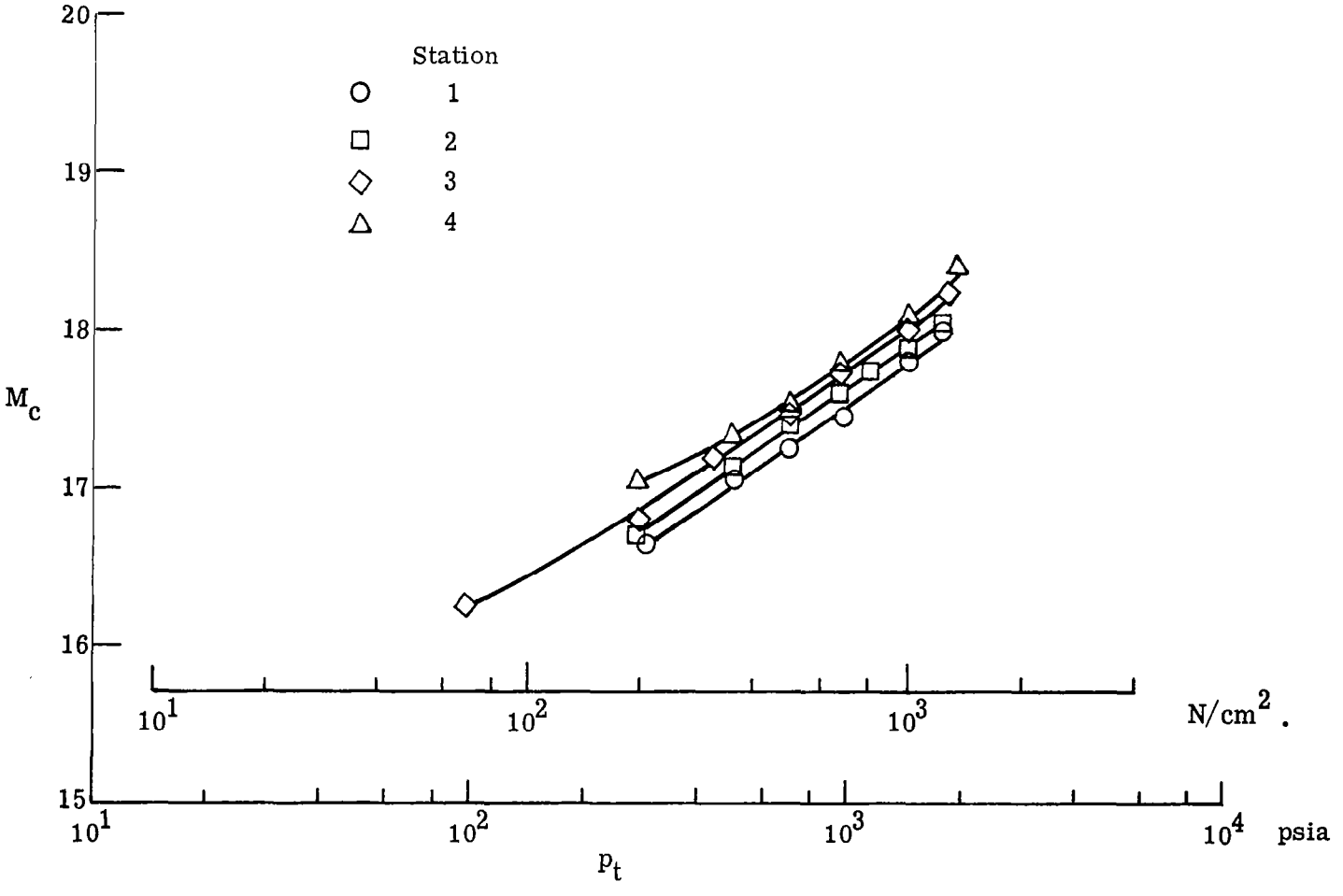

Figure 8.- Effect of stagnation pressure on average Mach number in test core.

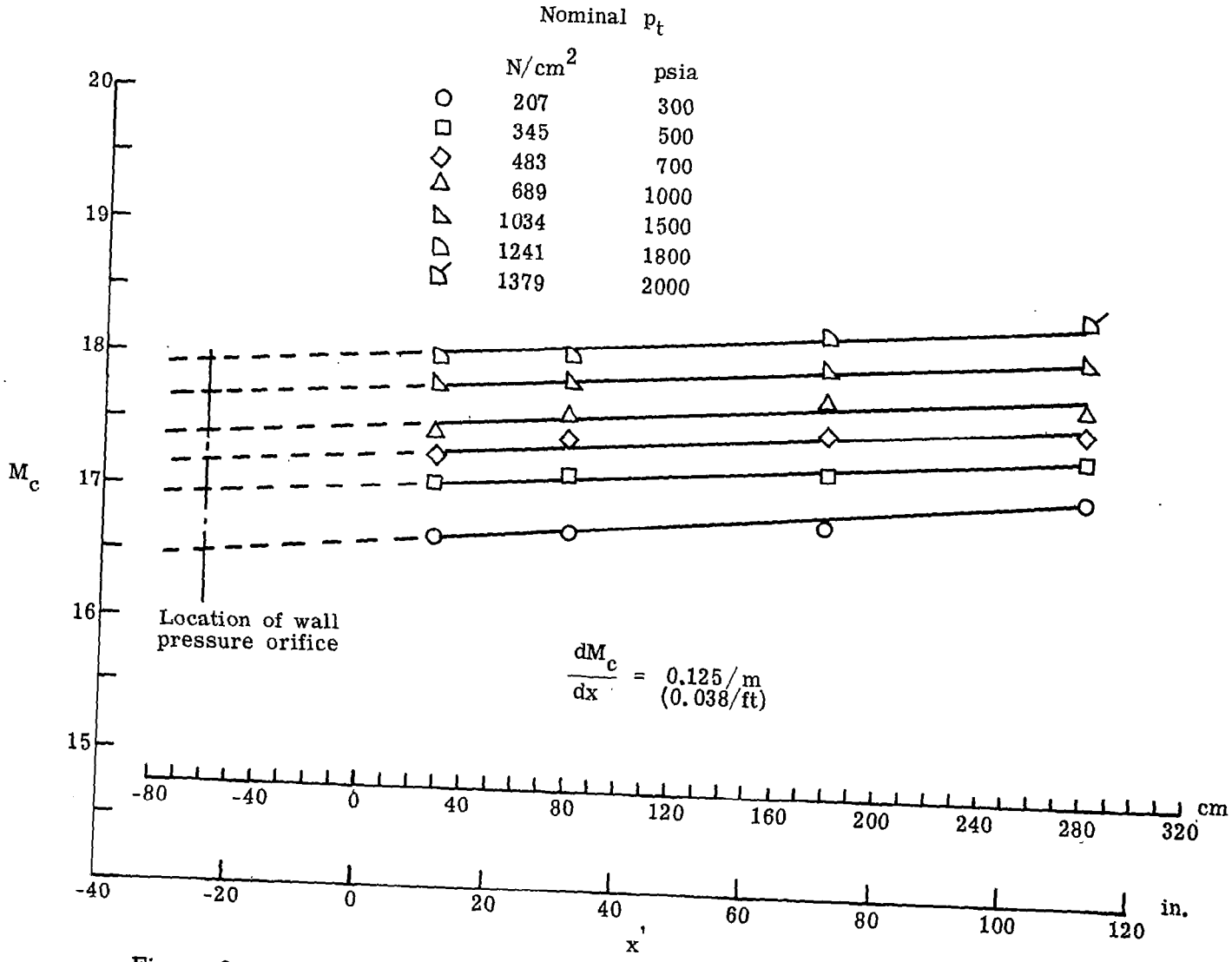

Figure 9.- Variation of average Mach number in test core with axial distance.

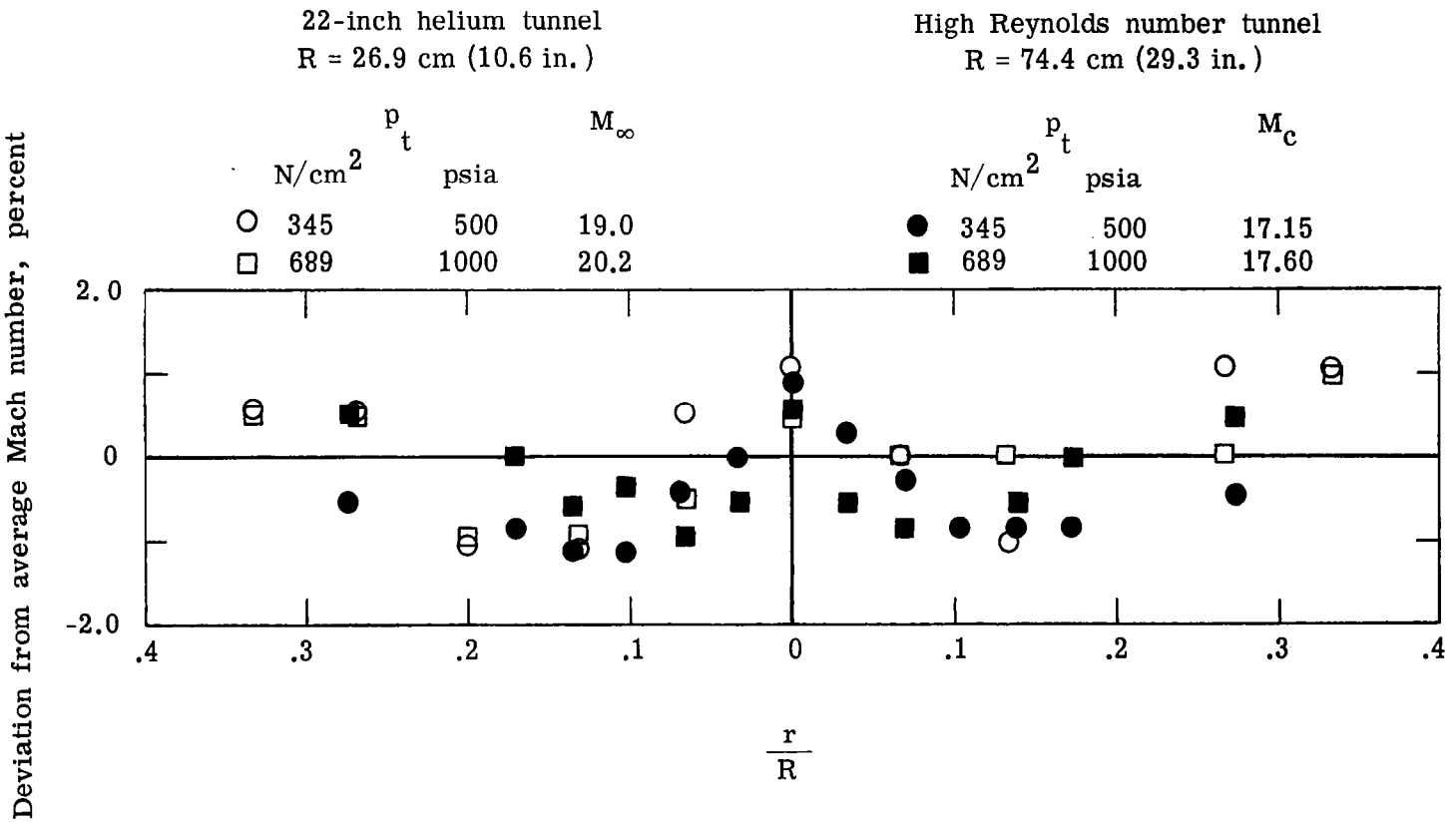

Figure 10.- Mach number distributions in the Mach 20 leg of the Langley high Reynolds number helium tunnel and the Langley 22-inch helium tunnel at x/d = 215.

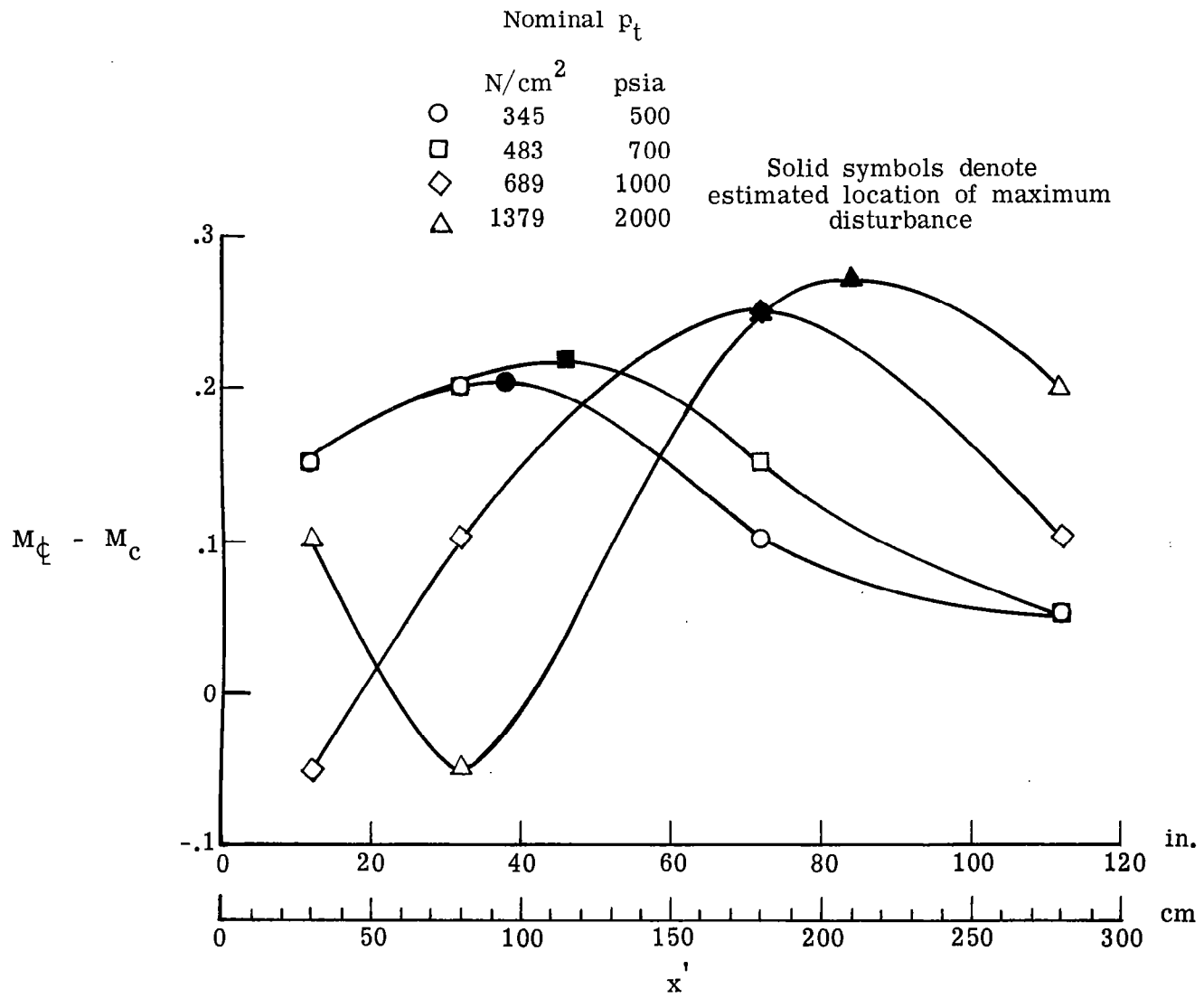

Figure 11.- Location of maximum center-line disturbances.

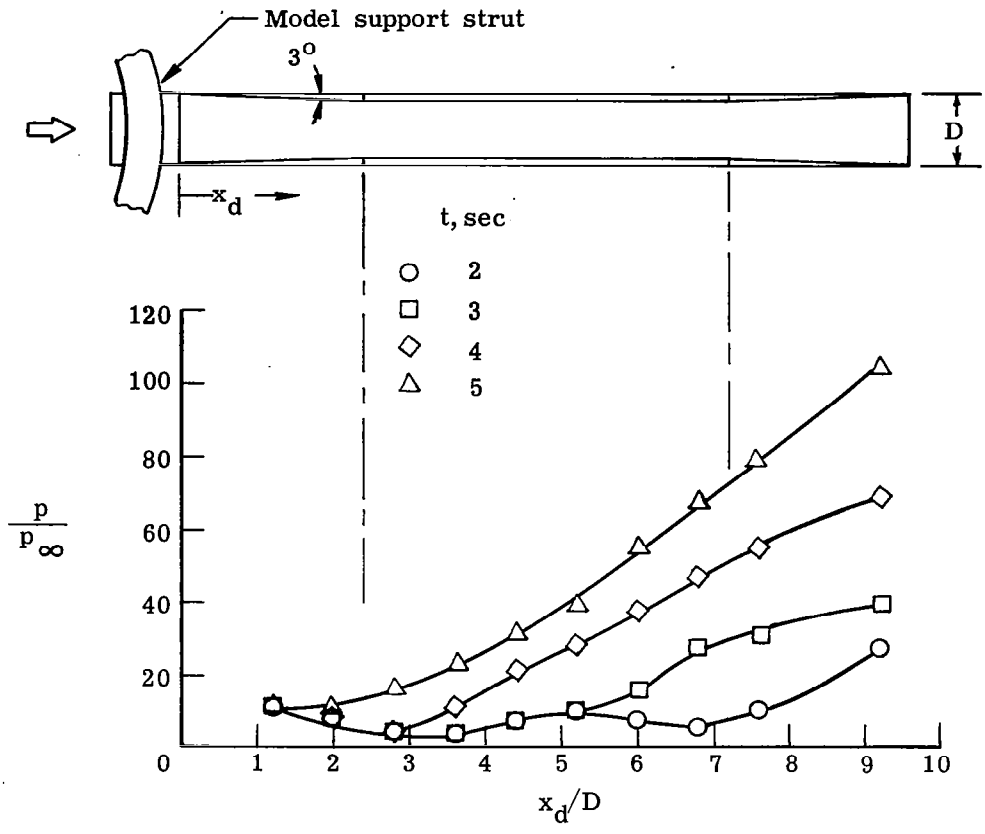

(a) Ratio of diffuser pressure to test-section static pressure.

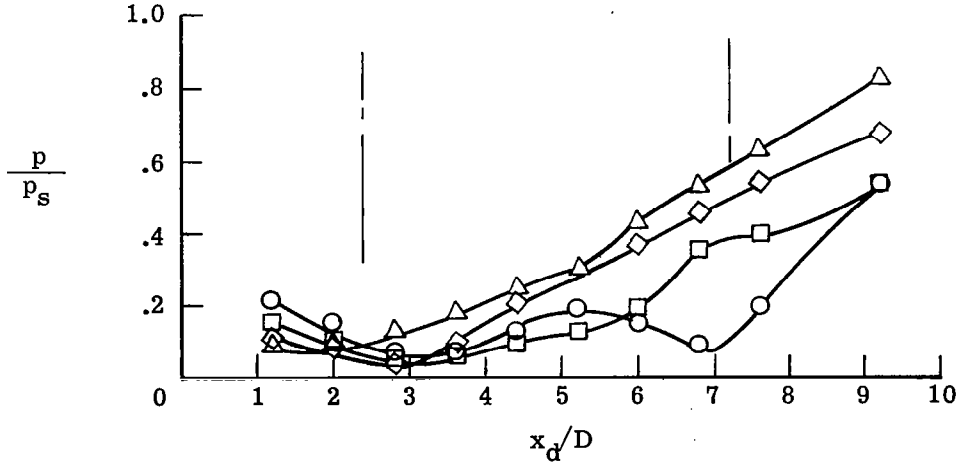

(b) Ratio of diffuser pressure to sphere pressure.

Figure 12.- Typical sphere and diffuser pressures. p_t = 689 N/cm^2 (1000 psia).

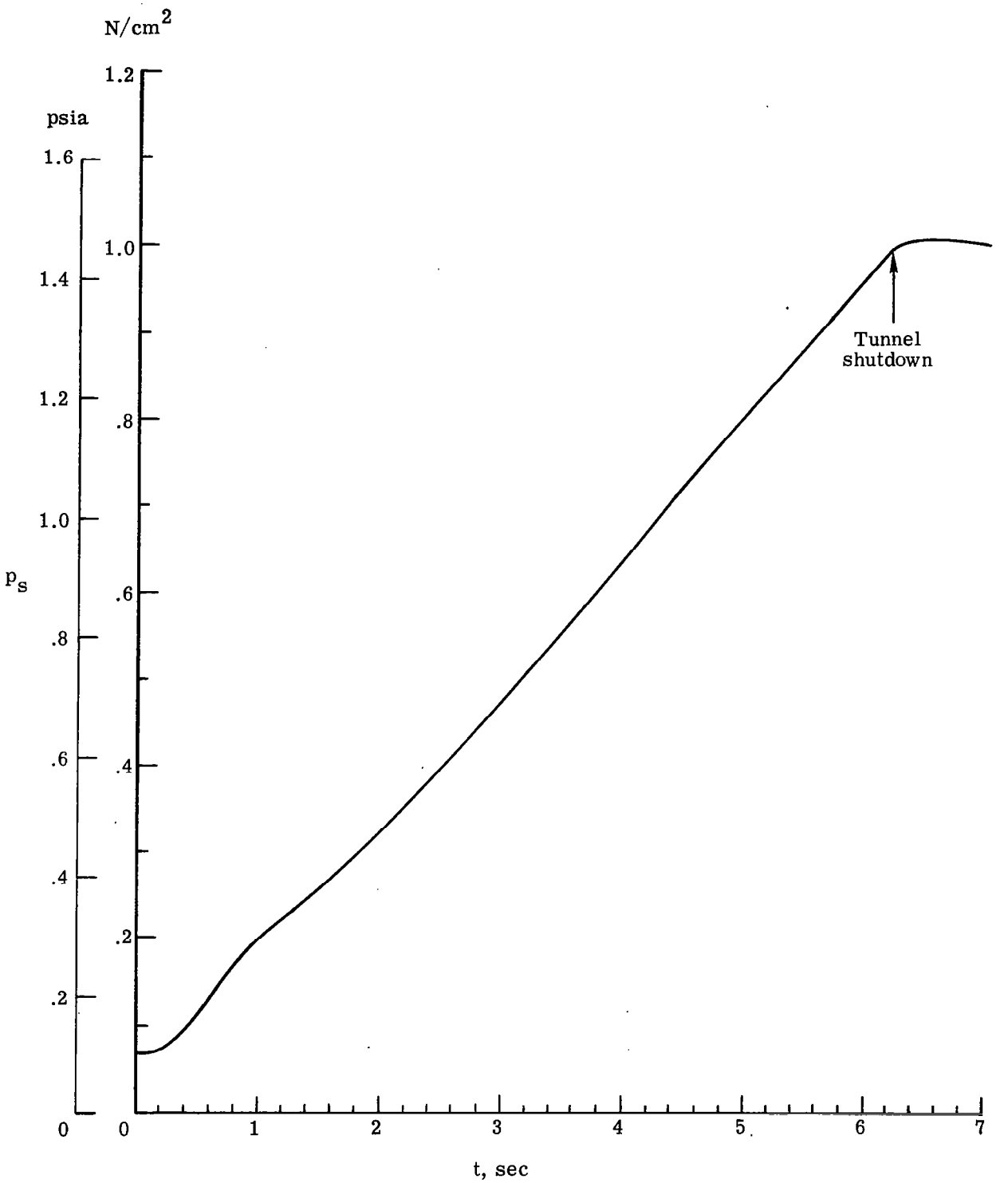

(c) Typical sphere-pressure variation during run.

Figure 12.- Concluded.

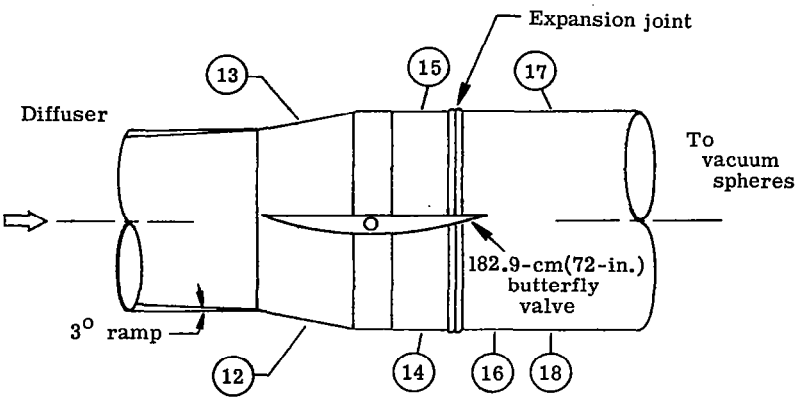

Location of pressure orifices near butterfly valve

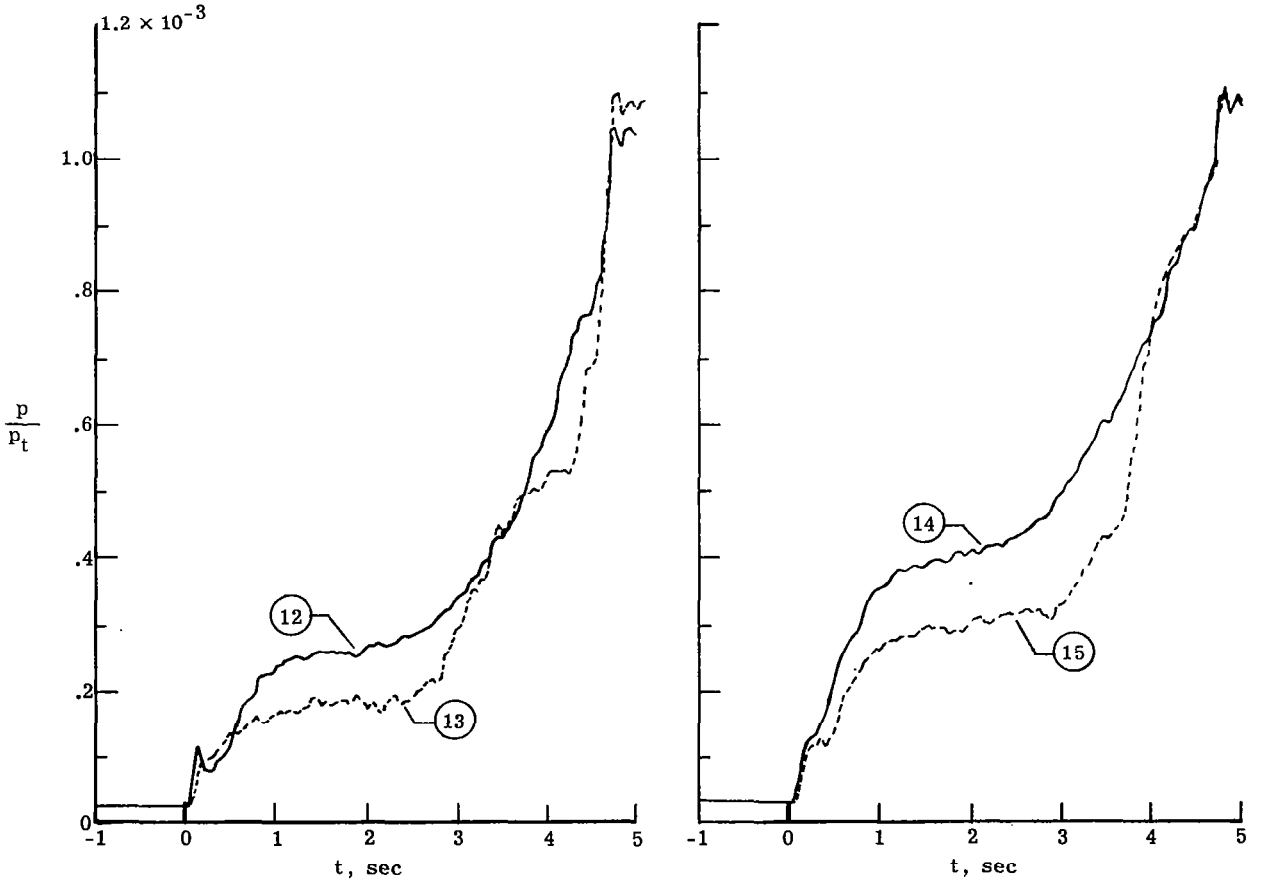

Figure 13.- Pressures at vacuum isolation valve.

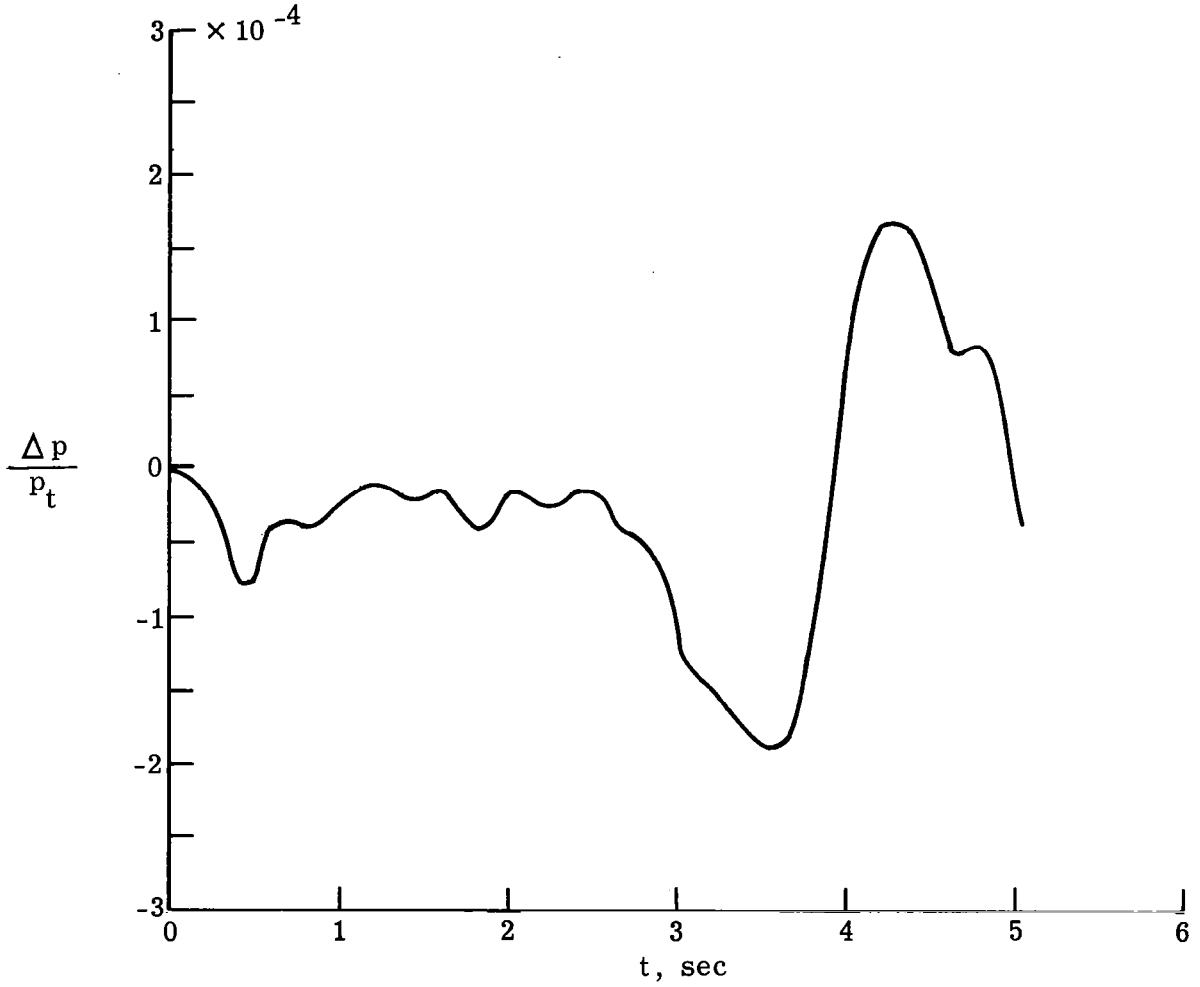

Figure 14.- Time-dependent pressure loading on vacuum isolation valve. p_t = 1236 N/cm^2 (1792 psia).

NASA-Langley, 1971 —— 11 L-7756

"The aeronautical and space activities of the United States shall be conducted so as to contribute . . . to the expansion of human knowledge of phenomena in the atmosphere and space. The Administration shall provide for the widest practicable and appropriate dissemination of information concerning its activities and the results thereof."

—NATIONAL AERONAUTICS AND SPACE ACT OF 1958

NASA SCIENTIFIC AND TECHNICAL PUBLICATIONS

TECHNICAL REPORTS: Scientific and technical information considered important, complete, and a lasting contribution to existing knowledge.

TECHNICAL NOTES: Information less broad in scope but nevertheless of importance as a contribution to existing knowledge.

TECHNICAL MEMORANDUMS: Information receiving limited distribution because of preliminary data, security classification, or other reasons.

CONTRACTOR REPORTS: Scientific and technical information generated under a NASA contract or grant and considered an important contribution to existing knowledge.

TECHNICAL TRANSLATIONS: Information published in a foreign language considered to merit NASA distribution in English.

SPECIAL PUBLICATIONS: Information derived from or of value to NASA activities. Publications include conference proceedings, monographs, data compilations, handbooks, sourcebooks, and special bibliographies.

TECHNOLOGY UTILIZATION PUBLICATIONS: Information on technology used by NASA that may be of particular interest in commercial and other non-aerospace applications. Publications include Tech Briefs, Technology Utilization Reports and Technology Surveys.

Details on the availability of these publications may be obtained from:

SCIENTIFIC AND TECHNICAL INFORMATION OFFICE

NATIONAL AERONAUTICS AND SPACE ADMINISTRATION

Washington, D.C. 20546